POOL BOILING STUDIES ON NANOTEXTURED SURFACES UNDER HIGHLY SUBCOOLED CONDITIONS

A Thesis

by

VIJAYKUMAR SATHYAMURTHI

Submitted to the Office of Graduate Studies of
Texas A&M University
in partial fulfillment of the requirements for the degree of

MASTER OF SCIENCE

December 2006

Major Subject: Mechanical Engineering

POOL BOILING STUDIES ON NANOTEXTURED SURFACES UNDER HIGHLY SUBCOOLED CONDITIONS

A Thesis

by

VIJAYKUMAR SATHYAMURTHI

Submitted to the Office of Graduate Studies of
Texas A&M University
in partial fulfillment of the requirements for the degree of

MASTER OF SCIENCE

Approved by:

Chair of Committee,	Debjyoti Banerjee
Committee Members,	N.K. Anand
	M. Sam Mannan
Head of Department,	Dennis O' Neal

December 2006

Major Subject: Mechanical Engineering

ABSTRACT

Pool Boiling Studies on Nanotextured Surfaces under Highly Subcooled Conditions. (December 2006)

Vijaykumar Sathyamurthi, B.E., Nagpur University, Nagpur, India

Chair of Advisory Committee: Dr. Debjyoti Banerjee

Subcooled pool boiling on nanotextured surfaces is explored in this study. The experiments are performed in an enclosed viewing chamber. Two silicon wafers are coated with Multiwalled Carbon Nanotubes (MWCNT), 9 microns (Type-A) and 25 microns (Type-B) in height. A third bare silicon wafer is used for control experiments. The test fluid is PF-5060, a fluoroinert with a boiling point of 56°C (Manufacturer: 3M Co.). The apparatus is of the constant heat flux type. Pool boiling experiments in nucleate and film boiling regimes are reported in this study.

Experiments are carried out under low subcooling (5 °C and 10 °C) and high subcooling conditions (20°C to ~ 38°C). At approximately 38°C, a non-departing bubble configuration is obtained on a bare silicon wafer. Increase in subcooling is found to enhance the critical heat flux (CHF) and the CHF is found to shift towards higher wall superheats. Presence of MWCNT on the test surface led to an enhancement in heat flux.

Potential factors responsible for boiling heat transfer enhancement on heater surfaces coated with MWCNT are identified as follows:

a. Enhanced surface area or nano - fin effect
b. Higher thermal conductivity of MWCNT than the substrate
c. Disruption of vapor-liquid vapor interface in film boiling, and of the "microlayer" region in nucleate boiling
d. Enhanced transient heat transfer caused by local quasi-periodic transient liquid-solid contacts due to presence of the "hair like" protrusion of the MWCNT
e. Enhancement in the size of cold spots
f. Pinning of contact line, leading to enhanced surface area underneath the bubble leading to enhanced heat transfer

Presence of MWCNT is found to enhance the phase change heat transfer by approximately 400% in nucleate boiling for conditions of low subcooling. The heat transfer enhancement is found to be independent of the height of MWCNT in nucleate boiling regime in the low subcooling cases. About 75%-120% enhancement in heat transfer is observed for surfaces coated with MWCNT under conditions of high subcooling in the nucleate boiling regime. Surfaces coated with Type-B MWCNT show a 75% enhancement in heat transfer in the film boiling regime under conditions of low subcooling.

To

My loving parents and sister

ACKNOWLEDGEMENTS

I would like thank my parents and sister for their constant encouragement in my educational pursuits.

I thank Dr. Debjyoti Banerjee for his guidance at various junctures of my research. I thank Dr. N.K. Anand and Dr. M. Sam Mannan for serving on my thesis advisory committee and providing me with enlightening comments on some aspects of this study which I had not considered before.

Further, I wish to thank Dr. Dennis O' Neal and Dr. Sai C. Lau and the Department of Mechanical Engineering at Texas A&M University for providing me with funds and resources towards fulfillment of my educational goals.

Special thanks are due to Dr. Ray Baughman, Dr. Mei Zhang and Dr. Shaoli Feng of the Nanotechnology Institute at University of Texas at Dallas for providing us with the test surfaces.

I thank Mr. Ysidoro Ramirez of the Heat Transfer Laboratory for providing me with equipment and timely assistance at various junctures of this endeavor. I thank Mrs. Yulia Vasilevya of the Materials Characterization Facility for the help extended with regard to training me in clean room equipment operation procedures.

I thank former and current lab members, especially Mr. Hee Seok Ahn, Mr. Sangwon Lee and Mr. Nipun Sinha, for providing me with valuable advice/suggestions.

TABLE OF CONTENTS

Page

LIST OF FIGURES

Page

Page

CHAPTER I

INTRODUCTION

1.1 Boiling Heat Transfer

One of the earliest results in the field of boiling heat transfer was published by Johann Gottlob Leidenfrost in 1756 [1]. Leidenfrost observed the rate of evaporation of water droplets on a red hot spoon. He observed that the droplets evaporated more rapidly at lower temperatures. This occurs due to a protective film of vapor that forms between the droplet and the heated surface at elevated temperatures leading to slower evaporation.

Pioneering experiments by Nukiyama [2] led to the inception of the boiling curve in 1934. Westwater and Santangelo [3] conducted a photographic study of the various regimes in pool boiling. They also measured the bubble departure diameters and frequencies from the high speed motion pictures they obtained. Hsu and Westwater [4] studied film boiling from vertical tubes. Since then, studies in the field of boiling heat transfer diversified. Studies have been carried out on bubble growth [5] and dynamics, hydrodynamic and thermal interactions between bubbles, thermal interactions between various sites, site activation, effect of pressure and

---

This thesis follows the style and format of the International Journal of Heat and Mass Transfer.

surface tension on heat transfer, temperature variations within the superheated boundary layer [6] and temperature variations within a bubble [7].

The effect of surface characteristics on the heat transfer coefficients is not yet well understood [8]. Thus, there exists a pressing need for more experimental data in this area. Surface characteristics such as roughness profoundly affect boiling processes. They provide sites for nucleation and cause an earlier incipience of boiling. In order to study the effect of surface structural features on boiling a number of studies have been carried out.

An enhanced structure consisting of six layers of grooved copper plates capable of being stacked was employed by Ramaswamy and co-workers [9] to investigate the effects of sub-cooling, pressure and height on its boiling performance. They concluded that subcooling and pressure caused an increase in the heat transfer rate. Furthermore, they studied the effect of varying pore size and pitch on boiling performance. It was observed that an increase in pore size and reduction in pitch augmented the heat transfer rate.

Coursey et al. [10] investigated the performance of graphite foam in nucleate boiling at various chamber pressures, working fluids and liquid levels. They concluded that heat fluxes approaching 50 W/cm^2 were attainable with wall temperatures maintained below 85°C.

Ujereh et al. [11] reported a 60% enhancement in the critical heat flux employing multi-walled carbon nanotubes (MWCNT) of 30 nanometer diameter and 20 – 30 microns length with FC-72 as the working fluid. The carbon nanotubes

(CNT) arrays were grown on a silicon substrate. However, the experimental uncertainty was not reported. Furthermore, the experiment was restricted to the nucleate boiling regime.

1.2 Carbon Nanotubes

CNT were first produced and analyzed using high resolution electron microscopy by M. Endo and others [12-14] in 1975. They analyzed the internal structures of carbon fibers produced by pyrolisis of Benzene and Ferrocene at 1000 °C. Both single walled and multi-walled carbon nanotubes (SWCNT and MWCNT) were imaged. Subsequently in 1991, S. Iijima [15] reported the formation of microtubules of graphitic carbon. MWCNT ranging from 4-30 nanometers in diameter and 1 micron in length were produced by using D.C. arc discharge evaporation in an argon filled chamber. The resulting structure was needle like and capped at one end.

Ever since their discovery, CNT have inspired tremendous research activities. Initially, research focused mostly on electrical properties of nanotubes [16]. However, as other properties such as their enhanced strength came to be discovered more potential applications emerged. For instance, CNT are amongst the stiffest known materials and this makes it useful for strengthening composites [17]. Hongjie Dai et al. [18] reported the use of carbon nanotubes to form AFM and STM tips for nanolithography.

Physical properties of CNT are dependent upon length, diameter and chirality. Furthermore, one can either have SWCNT or MWCNT. SWCNT can

exhibit either metallic or semi-conducting behavior based on its chirality and diameter [16-19]. The thermal properties of CNT are dependent upon its phonon dispersion relation and phonon density states [20]. CNT possess high thermal conductivity values (~3000 W/m°K). Their strong sp^2 bonds in conjunction with their rigidity and an almost atomic defect-free structure results in their unusually high thermal conductivity. The thermal conductivity of CNT varies with temperature and the phonon mean free paths. There is still disagreement with regard to the nature of variation of thermal conductivity of CNT with temperature in available literature [21-24].

1.3 Nanofluids

Whilst CNT have garnered a lot of attention in the past decade, nanofluids are beginning to interest researchers. Nanofluids are liquid suspensions containing a small amount of nano-particles which are found to enhance the thermal conductivity as compared to the base medium. Furthermore, the particles have at least one dimension in the 1-100 nanometer range [25]. Nanofluids possess higher thermal conductivities than those predicted by macroscopic theories [26-28]. They have been also shown to result in enhanced convective heat transfer [29], [30].

Nanofluids can be synthesized by using oxide nanoparticles, metallic nanoparticles or alternatively by carbon-nanotubes. While the high conductivity of CNT makes them ideal candidates for synthesizing nanofluids, rather conflicting results have been observed [25]. Theoretically, CNT with their high thermal conductivity and large aspect ratio should have a low percolation threshold.

However, this has not been realized in practice due to reasons that are not yet apparent. Some possible factors could be the tube to tube contact resistance, defects within the nanotubes and thermal interface resistance [31]. Thermal conductivity of CNT nanofluids are temperature dependent and increase non-linearly with particle loading [25]. Masuda et al. [32] reported a 30% enhancement in the thermal conductivity of water consisting of 4.3% by volume of Al_2O_3 nanoparticles 13 nanometers in size. Lee and others [33] observed only a 15% enhancement using Al_2O_3 nanoparticles 33 nanometers in size. Xie et al. [34] observed an intermediate result employing a particle loading of 5% by volume. A similar result was found by using SiC [35]. They reported an enhancement of 20% in their thermal conductivity values. A rather surprising 17% enhancement in thermal conductivity was reported by Wang and others [36] for a 0.4% volume loading of CuO in water. Eastman and co-workers [37] reported a 40% enhancement in the thermal conductivity of an ethylene glycol based nanofluid with a 0.3% by volume loading of 10 nanometer spheres of Cu.

Das et al. [38], initiated experiments on the boiling of nanofluids. You and others [39], observed a threefold increase in the critical heat flux using a nanofluid consisting of Al_2O_3 in water. Vasallo and co-workers [40] found a threefold increase in the CHF using silica in water nanofluid. Nanofluids show an increase in bubble departure diameters and a decrease in bubble departure frequency. Bang and Chang [41] used a nanofluid comprising of alumina nanoparticles (~ 47 nanometers average diameter) to observe the liquid film separating vapor bubbles from a heated

solid surface. Sefiane [42] investigated the role of structural disjoining pressure which arose from the ordered layering of nanoparticles in the confined wedge of an evaporating meniscus and the consequent pinning of the contact line. This pinning of the contact line is thought to hinder the spreading of dry spots thus causing a delay in the dryout hence leading to an enhancement in CHF.

1.4 Motivation for Study

The primary motivation for this study is to explore the nano-scale transport phenomena in boiling with applications in electronics chip cooling. Due to rapid increase in power densities in electronic chips in the past decade alternative cooling technologies are receiving an enhanced research interest. Phase change cooling is being considered as an alternative.

Based upon the heat fluxes encountered, Mudawar [43] classified applications as high heat flux (100 – 1000 W/cm^2) or ultra high heat flux devices (10^3 – 10^5 W/cm^2). Electronic components belong or will belong to the former category. Water being a polar fluid is unsuitable for cooling these electronic devices. Fluoroinerts, being dielectric fluids meet the electrical constraints required for these applications. However, fluoroinerts suffer from a severe drawback in that they have a low latent heat of vaporization. Therefore, techniques such as subcooling can be employed to enhance the heat transfer in nucleate boiling of fluoroinerts. Other approaches include using new materials/fluids such as CNT, nano-fluids, as well as nanotextured surfaces.

There exists the distinct possibility of achieving the requisite levels of cooling using CNT or nano-fluids. However, there is currently a paucity of studies in these aspects of boiling. Furthermore, the underlying mechanisms of heat transfer are still unclear in these cases.

1.5 Objective

The objective of this study is to experimentally measure the effect of nano-textured surfaces on the heat transfer rates under subcooled pool boiling conditions in the nucleate and film boiling regimes, particularly for the critical heat flux (CHF) condition in nucleate boiling and at the Liedenfrost point in film boiling.

1.6 Overall Scope

The experiments are conducted under moderate and highly subcooled pool boiling conditions. Saturation and subcooling levels of 5 °C, 10 °C , 20°C, 30°C and approximately 40°C (non- departing bubble condition) are studied.

Three different surfaces are used in this study. They are, bare silicon wafer, silicon wafer coated with Type-A MWCNT(9 microns height) and Type-B MWCNT (25 microns height). The MWCNT have diameters ranging from 8 to16 nanometers diameter. The nanotubes have a random pitch of 16-30 nanometers Ref. [44].

1.7 Overview

In chapter II titled, “Experimental Apparatus and Procedure”, details of the experimental apparatus and procedure will be outlined. In chapter III, calculations,

results and discussions shall be presented for the low subcooling and high subcooling pool boiling conditions. In chapter IV, conclusions from this study will be presented and the potential mechanisms for the nano – scale transport processes will be identified.

CHAPTER II

EXPERIMENTAL APPARATUS AND TEST PROCEDURE

2.1 Experimental Apparatus

Fig. 1 below (generated using Microsoft Visio®) depicts a schematic of the experimental setup. The experimental apparatus consists of the following:

1. A viewing chamber containing heat exchanger coil for pool boiling experiments.
2. A constant temperature bath for heating or cooling the test liquid.
3. A data acquisition system and power supply.
4. The test surface to be mounted on the heater apparatus.

A detailed description of each of the aforementioned components follows in the remaining sections. This is followed by an outline of the experimental procedure. The test procedure can be broadly categorized as follows:

1. Test surface installation.
2. Leak testing.
3. The degassing step.
4. Data collection.

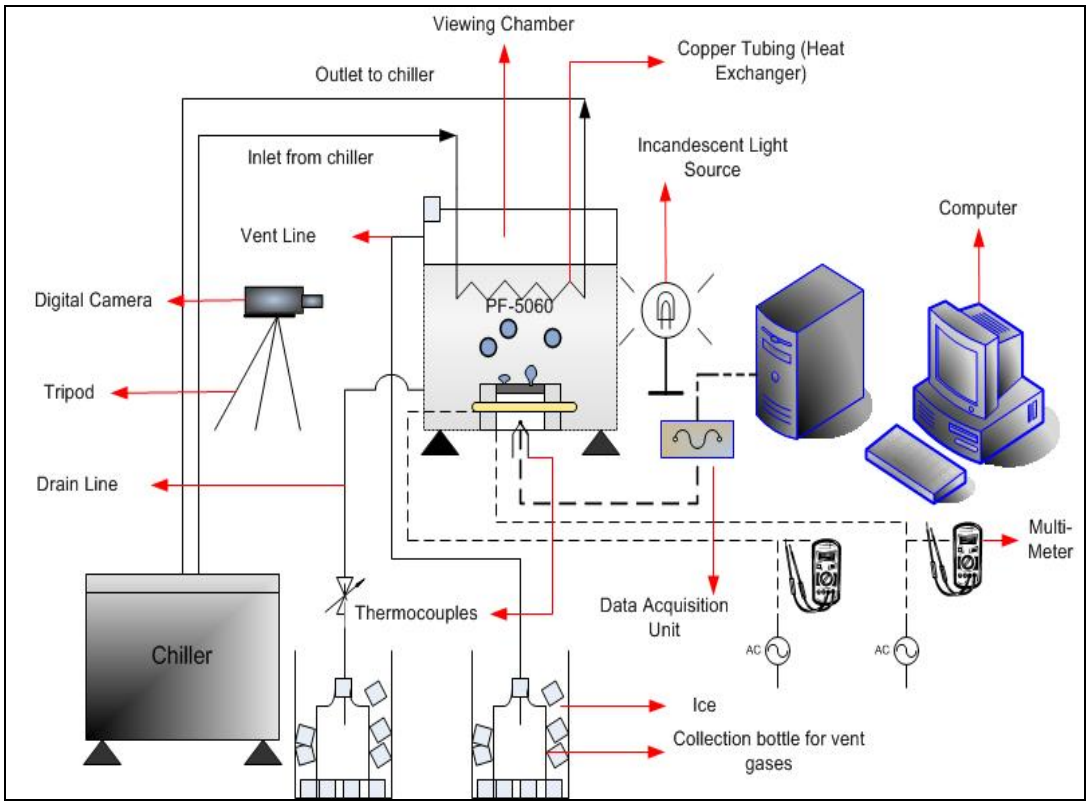

Fig. 1. Schematic of the test setup (Not to scale).

2.2 Details of Experimental Setup

a) *Viewing Chamber:* The viewing chamber functions as a test chamber (Help by Mr. Hee Seok Ahn, graduate student, Texas A&M University, in construction of the viewing chamber apparatus is gratefully acknowledged). It is transparent on three sides allowing visual access and acquisition of digital images of the test in progress.

Fig. 2 (generated in SolidWorks®) shows the construction of the viewing chamber.

The viewing chamber consists of a skeletal structure comprising of twelve 1/8 inch thick and 1 inch wide steel L-beams. The L-beams are welded together to form a structure, cubical in shape. Two steel plates are welded to the bottom and one adjacent side of this structure. The

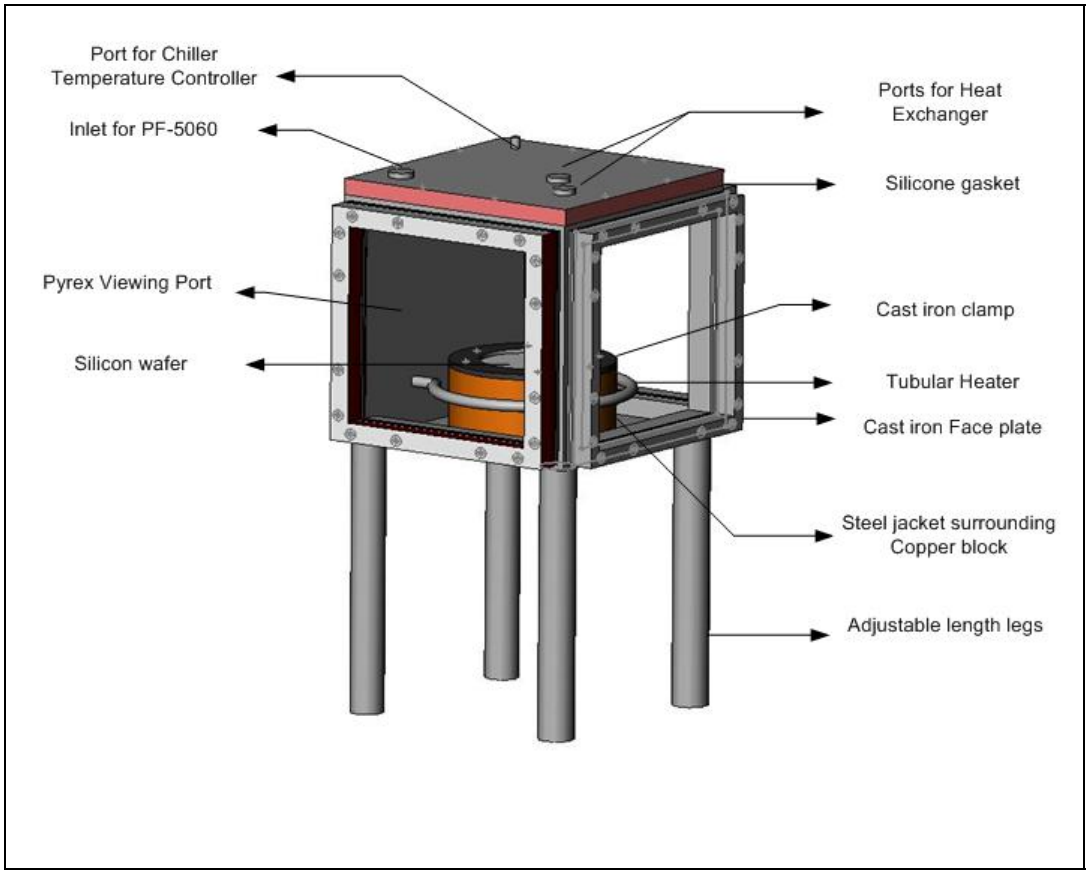

Fig. 2. Viewing chamber construction (not drawn to scale).

steel plate at the bottom has a hole drilled in it. This allows the power lines to the cartridge heaters and thermocouple lead wires to pass through. The steel plate on the side has two holes drilled for the tubular heater and its power supply connections. These aside there are two more holes approximately 0.5 inches in diameter provided on the same plate for venting the chamber (located 1.125 inches from the top) and for draining the test liquid (located 0.125 inches from the bottom). The vent line also ensures constant atmospheric pressure within the test chamber. A detachable steel plate is used as a cover plate for the top of the viewing chamber. It has four holes drilled in it. Two holes allow the cooling coil inlet and exit tubes to pass through from within the viewing chamber for connecting to the constant temperature bath. One of the holes is used to pour the test liquid into the viewing chamber. The other hole is used to insert the chilling unit's temperature sensor. The remaining three sides of the viewing chamber are enclosed by Pyrex glass which is placed between two 0.125 inch thick silicone sheets. The silicone sheets are cut, so as to provide a transparent square viewing region measuring 4.5 inches × 4.5 inches. This is attached to the steel framework of the viewing chamber on one side and a specially cut steel frame (with a 4.5 inches × 4.5 inches viewing area) on the other side by means of

screws. Additionally, the silicone gaskets prevent the Pyrex from cracking due to differential thermal stresses. A leak proof enclosure is thus formed.

The viewing chamber houses a copper block (Fig. 3) measuring 3.5 inches in diameter and 2.5 inches in height. The copper block is 99% pure and is deoxidized. It houses five cartridge heaters. Three cartridge heaters are rated 500 Watts and two are rated at 300 Watts (Manufacturer Watlow Inc.). Twelve calibrated, sheathed, K - type thermocouples are located at various radial locations at depths of 0.1250 inch, 0.3750 inch, 0.6250 inch and 0.8750 inch. There are three thermocouples at each level. Six holes are provided at the bottom of the copper block to affix it to the welded steel plate at the bottom using screws. The copper block is surrounded by an annular steel jacket with a 3.9 inch internal diameter, a 4.5 inch external diameter and 1.97 inch height. An air gap is enclosed between the steel jacket and the copper block. Air being a poor conductor acts as a thermal insulator preventing excessive heat loss from the sides of the copper block. This arrangement also prevents the power supply and thermocouple lead wires from contacting the test liquid directly. Six holes are drilled and tapped into the steel jacket for mounting it on the bottom steel plate using screws. Six holes are drilled and tapped at the top of the

jacket for mounting a clamp. The test surface is mounted using a clamp. The steel clamp is attached to the steel jacket using screws. A Teflon gasket is placed between the clamp and the test surface.

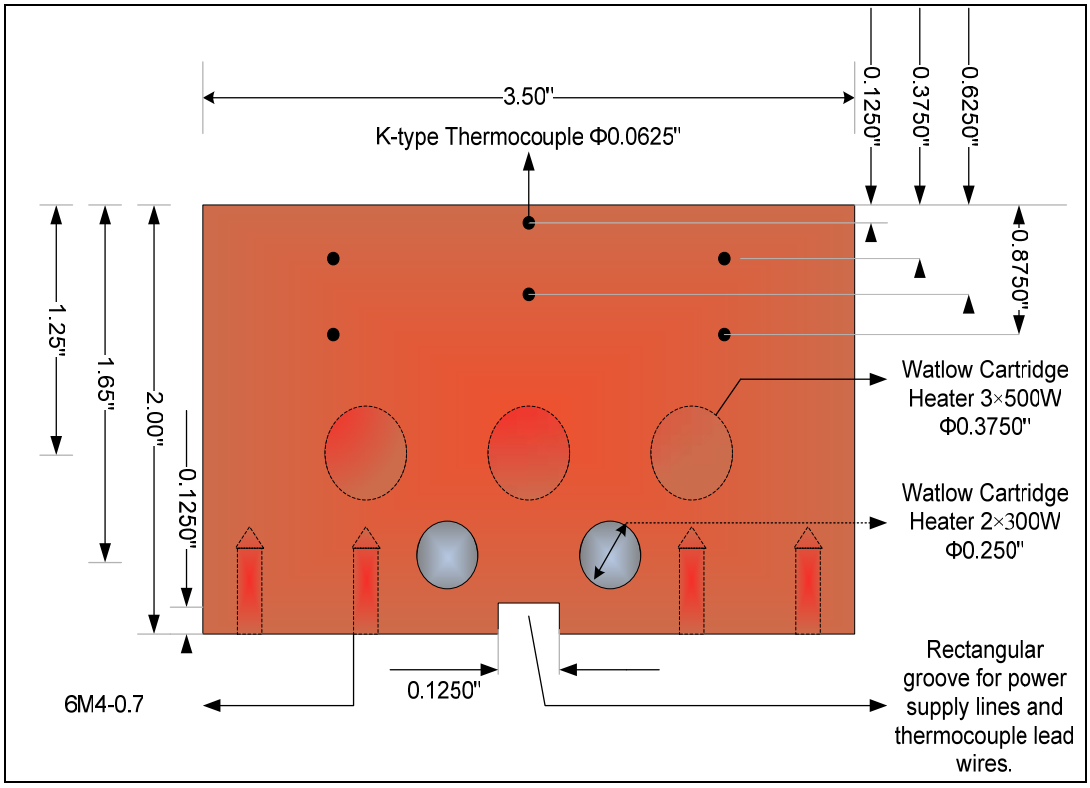

Fig. 3. Copper block schematic (not drawn to scale).

Silicone gaskets are present between the clamp and steel jacket to ensure a leak proof system. Fig. 4 below is a digital image of the viewing chamber.

Two collection bottles are placed in containers filled with ice. One is to collect the drained test liquid. The second serves to condense the vapor generated during degassing and during the experiments.

b) *The Constant Temperature Bath and Cooling Coil:* The constant temperature bath (Manufacturer: Polyscience®, Model: 9612, Pump: 5- speed duplex), depicted in Fig. 5, consists of a bath with the working fluid, a pump, a refrigeration system and a programmable controller (RS232 interface). The working fluid is a mixture of 10% ethylene glycol and water. The working fluid is maintained at a constant temperature.

The working fluid is pumped through tubes into the heat exchanger coil located within the viewing chamber. This heat exchanger coil then transfers heat into or absorbs heat from the test liquid thus maintaining it at a constant temperature. The temperature of the test liquid is monitored by one or two K-type thermocouples. Two thermocouples are used in the non – departing configuration.

Two different cooling coils are used in the experiments. Both cooling coils are made from a 0.25 inch diameter copper tubing using a tube bender. For experiments with high cooling loads, (e.g. non – departing bubble configurations), the cooling coil with a higher capacity was used.

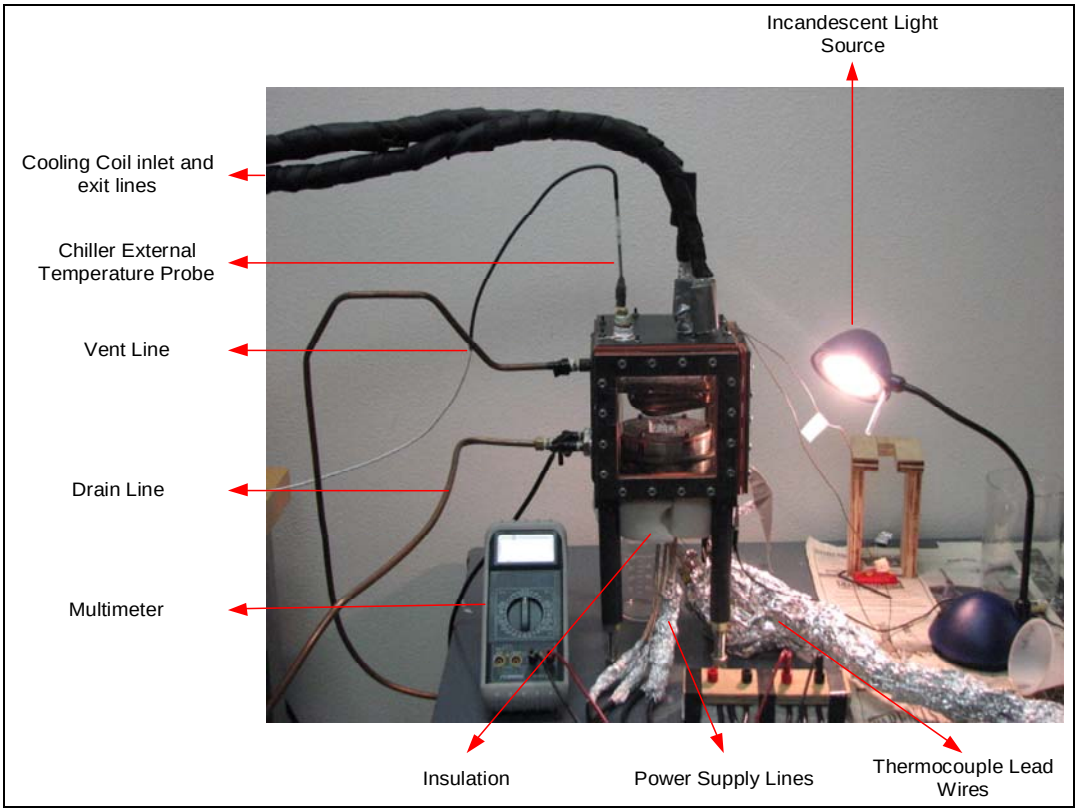

Fig. 4. Photograph of the viewing chamber and some other test components.

c) *Data Acquisition System and Power Supply:* The data acquisition system shown in Fig.6 comprises of a National Instruments SCXI - 1000 chassis with a SCXI – 1303 terminal block, analog MUX (32-channel Thermocouple Amplifier modules), and PCI-6251 DAQ board with a Pentium – 4, 3.2 GHz computer and LABVIEW 7.1 software.

A handheld multimeter (Manufacturer: Omega ®, Model: HHM 14, True RMS multimeter, Frequency response: up to 20 KHz, 0-750

V, ± 1.5 % 50 – 20 KHz) is used to record the supply voltage to the cartridge heaters.

An AC/DC clamp meter (Manufacturer: TENMA, Model: 72-6185, True RMS, AC current: 4, 40, 100, 400A, Frequency: 100 Hz – 100 KHz) is used to measure the current supplied to the five cartridge heaters.

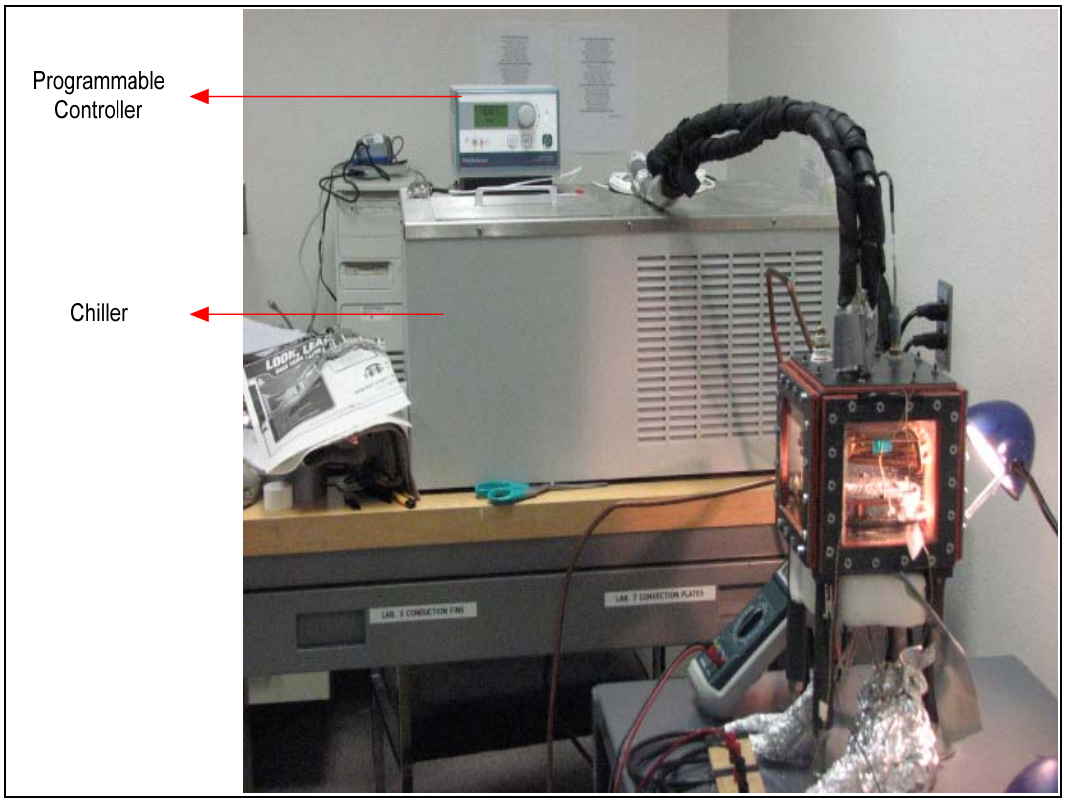

Fig. 5. The Polyscience®, constant temperature bath.

A variable transformer (Manufacturer: Staco Energy Products Co., Model: 3PN2210B, Series: 2200, Input: 120 Volts AC, Frequency: 50-60 Hertz, Output: 0-140 Volts) is connected to the cartridge heaters within the copper block and provided the requisite power level.

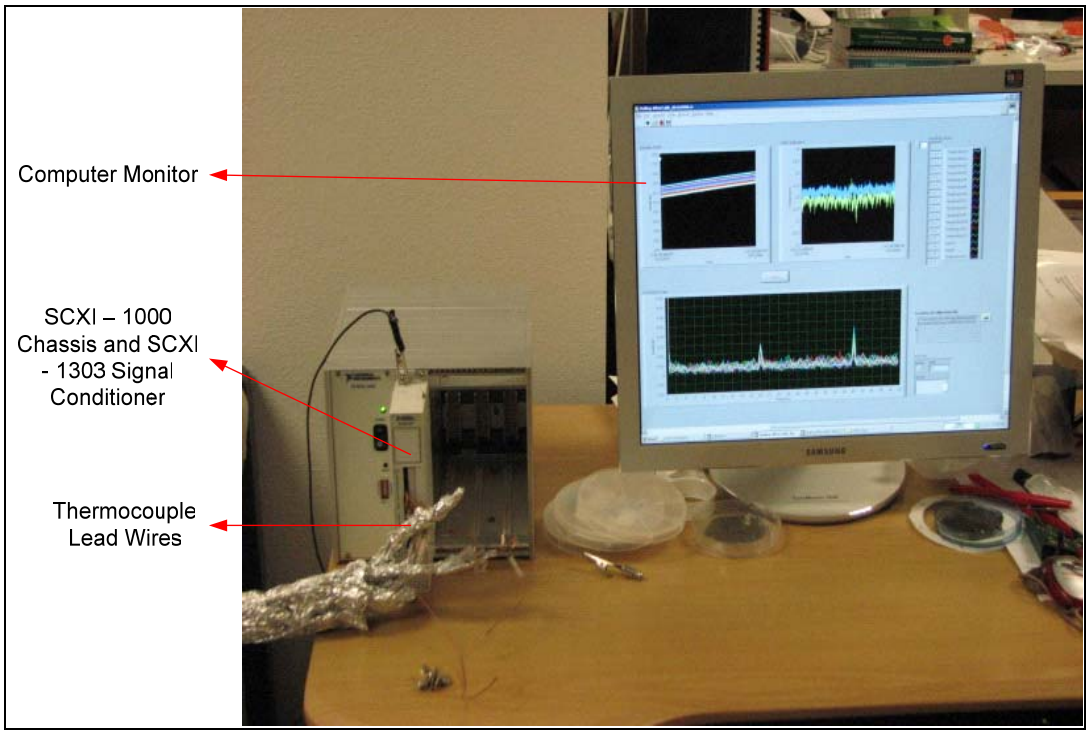

Fig. 6. Data acquisition system and digital display used for real-time temperature monitoring.

d) *Test Surface:* Three different test surfaces are used. The base (substrate) of the test surfaces consists of 3-inch silicon wafer (Supplier: University Wafers, Doping: P-type (100)). Two test

surfaces are obtained by coating the substrate with MWCNT of two different heights (Fig. 7.). The MWCNT is grown by Chemical Vapor Deposition (CVD) on a silicon substrate. A 5 nanometer thick layer of iron is deposited by e-beam evaporation on the substrate. This serves as a catalyst for the synthesis of MWCNT. Acetylene is flown (5 mole percent concentration) in a quartz tube maintained at a temperature of 680 °C, at a rate of 580 sccm in Helium and at atmospheric pressure. The synthesis time ranges from a few seconds to 10 minutes. The growth rate is of the order of 1 - 2 microns per second. Vertically aligned MWCNT are obtained by this process. Their diameters range from 8 – 16 nanometers. The MWCNT are 9 microns (Type – A) and 25 microns (Type - B) in height. The purity of this process is high (~ 96 – 98 % carbon present as MWCNT, 2 – 4 % amorphous carbon and iron). The MWCNT have a random pitch of 16 – 30 nanometers. Further details of the process can be found in [44], [45].

(The author would like to acknowledge the help of Dr. Ray Baughman Dr. Mei Zhang and Dr. Shaoli Feng of the Nanotechnology Institute at University of Texas at Dallas for providing us with the test surfaces.)

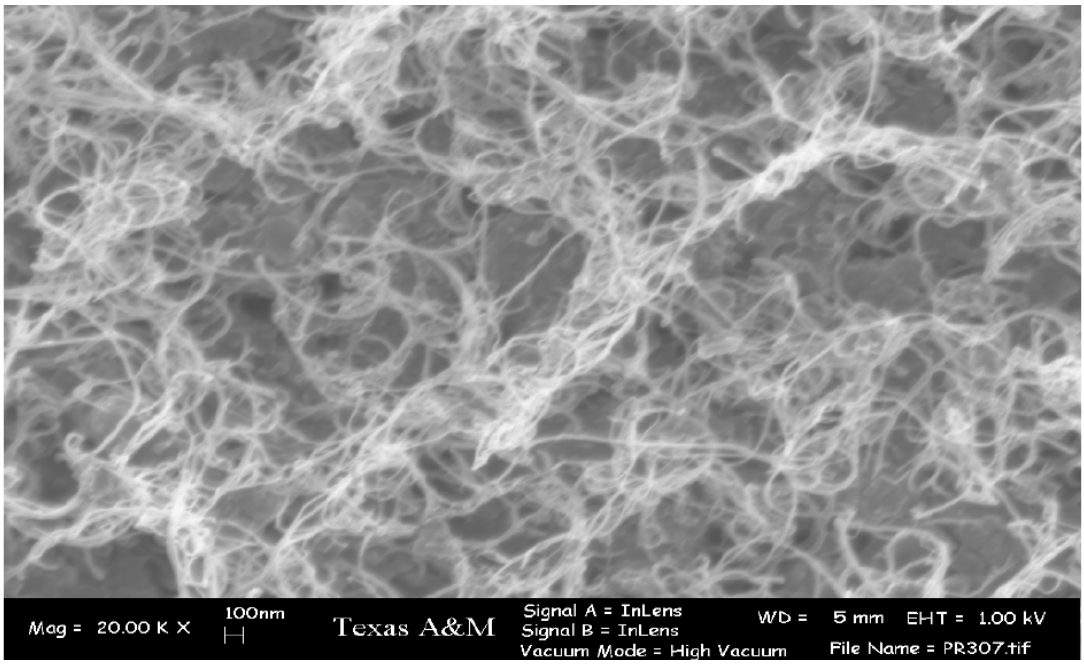

Fig. 7. Scanning electron micrograph of Type-A CNT coated test surface as viewed from top.

2.3 The Experimental Procedure

The actual pool boiling experiments comprise of the degassing step and the subsequent data acquisition step. The experimental duration (comprising of the above mentioned steps) varies from 13 hours (Type – B, high subcooling) to approximately 30 hours. The entire test procedure is outlined below.

a) *Test Surface Installation:* A layer of Dow Corning 340, silicone heat sink compound is applied on top of the horizontal surface of the copper block. A 3 – inch Pyrex wafer is placed on top of the copper block. Another layer of heat sink compound is applied on top of the Pyrex wafer. The silicon wafer is then placed on top of the Pyrex

wafer. A Teflon sheet is then cut and fixed onto the underside of the steel clamp using silicon glue. After curing the silicon glue (~ 45 minutes), the clamp is fixed on the steel jacket using screws. A uniform tightening torque is applied on the screws by using a torque wrench. The Teflon sheet underneath the clamp is used to prevent any damage to the wafer surface.

b) *Leak Test:* After clamping, a leak test is performed using deionized (DI) water. If a leak is detected the screws are tightened gradually. In most cases a torque greater than 5.2 N-m is unacceptable as it causes the wafer to crack either immediately or during the test as a result of thermal stresses. Typical torques used range from 3 – 4.4 N-m.

c) *Degassing Step:* Once the leak test is performed the apparatus is allowed to dry for a day. The cooling coil is lowered into the viewing chamber and top steel plate is clamped using screws, on the viewing chamber framework. Prior to start of the actual experiment a degassing step is performed. This is done to remove the trapped gases within the test fluid and to prevent premature nucleation. The bulk test fluid is heated to its boiling point and maintained at that temperature for 20 minutes. The test fluid in this case is PF – 5060 (Manufacturer: 3M Co., Boiling Point: 56°C).

d) *Data Acquisition:* After degassing is performed, depending upon the nature of experiments performed (saturation or subcooling) the

cooling coil is either placed above the test fluid (saturation experiments) or immersed (subcooling experiments) in the test fluid. The temperature of the chilling unit is fixed to achieve a desired temperature level of the test fluid. The tubular heater power supply is disconnected (for subcooling cases). Power supply to the cartridge heaters is modulated by the variac. The system is allowed to reach steady state for each power setting. The temperature of the test fluid is carefully monitored in LABVIEW® and adjustments to the chiller temperature level are made accordingly during the time taken to reach steady state. The temperatures within the copper block are also monitored continuously in LABVIEW®.

Once steady state is achieved, the DAQ system is used to record the thermocouple readings for a period of two minutes at a rate of 200 Hz. The temperature readings are used to evaluate the heat flux and wall superheats. These are then used to construct the boiling curve for PF – 5060. The current and voltage supplied to the cartridge heaters are recorded manually using the clamp type ammeter and multimeter respectively. In addition the chiller temperature and time is recorded. A Canon® S3 IS digital camera is used to capture digital images after steady state conditions are reached. The power supplied is increased in steps of 3 or 5 volts and the aforementioned data acquisition procedure is repeated.

CHAPTER III

RESULTS AND DISCUSSIONS

3.1 Estimation of Wall Temperature

The temperature profile within the copper block is used to evaluate the heat flux. Fourier's law of one dimensional heat conduction is used. The equation used is:

$$q'' = -k\frac{\Delta T}{\Delta x} = -k\frac{(T_2 - T_9)}{\Delta x} \tag{3.1}$$

Wherein, *q"* represents the heat flux, *k* represents the thermal conductivity of the copper block, ΔT represents the gradient of the scalar temperature field within the copper block between the two thermocouples and Δx the distance between the two vertically aligned thermocouples. T_2 and T_9 are temperature values recorded by two thermocouples inserted in the copper block aligned in the same vertical plane.

The thermal resistance between the copper block and the test surface is measured experimentally. Thin film thermocouples (TFT) [46], [47] are used to obtain the surface temperature during pool boiling experiments. Mechanically reinforced wire bonding techniques using JB weld are used to package the TFT (Manufacturer: J-B Weld Co.). The thin film thermocouples are calibrated using a standard K - type thermocouple in air. The K – type thermocouple is calibrated using a NIST thermometer by placing them in a constant temperature bath. The K-type thermocouple is attached using JB weld to the wafer containing TFT. The

curing time is approximately 24 hours. TFT junctions have minimal interference on the boiling process compared to bigger wire bead thermocouples. It must be noted that the wire-bead K - type thermocouples are not capable of accurately estimating the surface temperature in boiling conditions. This is due to their relatively large junction size as compared to a TFT junction and in many cases improper contact with the silicon wafer surface or small contact area. This would therefore lead to a large error in the measured value of wall superheat. Furthermore, significant nucleation occurs at the bond site leading to a local decrease in temperature. Hence, in order to minimize the errors in surface temperature estimation, calibration of the TFT is carried out using the K – type thermocouples in air. Air, having a low convective heat transfer coefficient and by virtue of being a good thermal insulator leads to a more uniform temperature field surrounding the (relatively large) K – type thermocouple junction.

Some studies [48-51] have employed hot-wire anemometry to measure void fractions and artificial cavity interactions [52] in two phase flow. However, it has also been noted in literature [53] that bubbles smaller in diameter than the probe diameter tends not to strike the probe surface. Bubbles with a diameter larger than the probe diameter and length greater than that of the probe tend to behave unpredictably. Furthermore, film boiling may occur on the surface of the probe. This aside, it is difficult to mount the probes flush with a silicon surface. In addition the TFT junctions have smaller overall form factor than the cylindrical probe

leading to a quicker response. Moreover, it is relatively easier to make TFT on silicon wafer using micro – fabrication techniques (Ref. [54]) techniques.

After calibration of the TFT, a pool boiling experiment is carried out. Typically, this is either in saturation or 10 – degree subcooled pool boiling conditions. The experimental procedure mentioned in the previous chapter is followed. Once the surface or wall temperature is obtained, the thermal resistance is estimated from the following equation:

$$R_{th}'' = \frac{T_{Cu} - T_w}{q''} \tag{3.2}$$

In the above equation, R_{th}" is the effective thermal resistance between the top of the copper block and the top of the silicon wafer on a unit area basis. The wall temperature T_w, is also affected by the effective boiling heat transfer from the surface. Therefore, this resistance intrinsically accounts for the effective boiling heat transfer coefficient for different regimes of boiling. Typically, however, effective boiling heat transfer coefficients range from 700 – 1000 W/m^{2}K (Ref. [47]), resulting in very little impact on the thermal resistance value. *Tw*, T_{Cu} represents the surface temperature and the temperature at the top of the copper block respectively. Here, q" is the wall heat flux. A correlation between the copper block temperature (at the top) and the wall temperature is thus obtained from the pool boiling experiments for both, the nucleate as well as film boiling regimes. For this study the following correlations are used for the nucleate and film boiling regimes (help of Mr. Ahn is acknowledged in obtaining the following correlations):

$$R_{th} = \frac{0.702961}{1+\left(\frac{T_{Cu}}{60.56}\right)^{-6.808}} \tag{3.3}$$

$$R_{th} = 0.321873 + 3.783\times10^{-3} T_{Cu} \tag{3.4}$$

The wall temperature is then estimated from the following equation:

$$T_w = T_{Cu} - q'' R_{th''} \tag{3.5}$$

In evaluating the wall temperature using these correlations, the test surface area exposed to the test liquid, denoted by A_e is used.

3.2 Estimation of Uncertainty

The uncertainty in heat flux is evaluated using the Kline and Mc-Clintock [55], procedure. The resulting expression for the relative uncertainty in heat flux is:

$$\frac{\omega_{q''}}{q''} = \sqrt{\left(\frac{\omega_k}{k}\right)^2 + \left(\frac{\omega_{T2}}{T_2 - T_9}\right)^2 + \left(\frac{\omega_{T9}}{T_2 - T_9}\right)^2 + \left(\frac{\omega_{\Delta x}}{\Delta x}\right)^2} \tag{3.6}$$

Where, ω denotes the uncertainty in the particular quantity indicated by the subscript. The thermal conductivity of copper is taken from the standard tables to be 398 W/m°K. The relative uncertainty in the thermal conductivity is ± 1%. The relative uncertainty in the positioning of the thermocouples is ± 3%. The magnitude of uncertainties in the temperatures T_2 and T_9 is determined using a 95% confidence and steady state temperature readings.

3.3 Results and Discussion

Experiments are carried under saturation, at 5 ºC and 10 ºC subcooling corresponding to low subcooling as well as at 20 ºC and 30 ºC corresponding to

high liquid subcooling. Tests are also carried out at ~ 37 ºC subcooling resulting in the non-departing or static bubble condition. The test surfaces for the first four cases are bare silicon wafer, silicon wafer with Type – A CNT and silicon wafer with Type – B CNT. For the static bubble condition test surfaces used are bare circular silicon wafer and silicon wafer with Type-A CNT. Each test is repeated at least twice to ensure repeatability.

a) *Low Subcooling Cases:* Fig. 8 depicts the results for the saturation and low subcooling cases with error bars (Mr. Hee Seok Ahn's help in setting up the apparatus and acquisition of data in some of the low subcooling experiments is acknowledged and greatly appreciated. The saturation and 10-degree subcooling data for type-A CNT as well as the saturation data for type-B CNT has been reproduced from [46]). Fig. 9 shows the pool boiling curves for the second set of runs corresponding to the low subcooling regime. It is observed that the heat transfer is enhanced due to the presence of the CNT by 30 – 300% compared to the bare silicon surface.

The height of the CNT seems to be a less dominant factor in the heat transfer enhancement in the nucleate boiling regime. Heat transfer rates in the nucleate boiling regimes are dependent on the number and size of nucleation sites. Both Type – A and Type – B CNT probably provide similar number of nucleation sites, significantly higher than the bare silicon surface. In sharp contrast

however, the film boiling regime shows a high degree of sensitivity to the height of microstructures. Type – B CNT shows a markedly higher heat transfer in the film boiling regime than either the Type-A CNT or the bare silicon wafer for the same level of subcooling. This could possibly be due to the local rupture of the vapor film at points of minimum thickness, resulting in a transient quenching of the substrate by the test liquid, thus improving heat transfer rates. The observed facts are consistent with observations from numerical and experimental studies in existing literature [55-57]. These studies have shown the dynamic film thickness to range between 15 and 20 microns. Thus, Type – B CNT could disrupt the vapor film by virtue of its length, in the film boiling regime. The enhanced heat transfer in the nucleate boiling regime could be a result of the disruption of

the liquid microlayer underneath the bubbles. Another factor could be the pinning of the contact line by the microstructures.

Subcooling is found to enhance the heat transfer at points close to the CHF. Furthermore, subcooling causes the CHF to shift towards higher wall superheats. Subcooling is also found to cause a shift in the Liedenfrost points towards higher wall superheats. Within the bounds of experimental error, Type - A CNT seems to result in a slightly higher heat transfer as compared to Type - B CNT in the nucleate boiling regime. For a given level of subcooling, Type - B CNT shows a higher heat transfer at CHF and also tends to shift the CHF towards higher wall superheats.

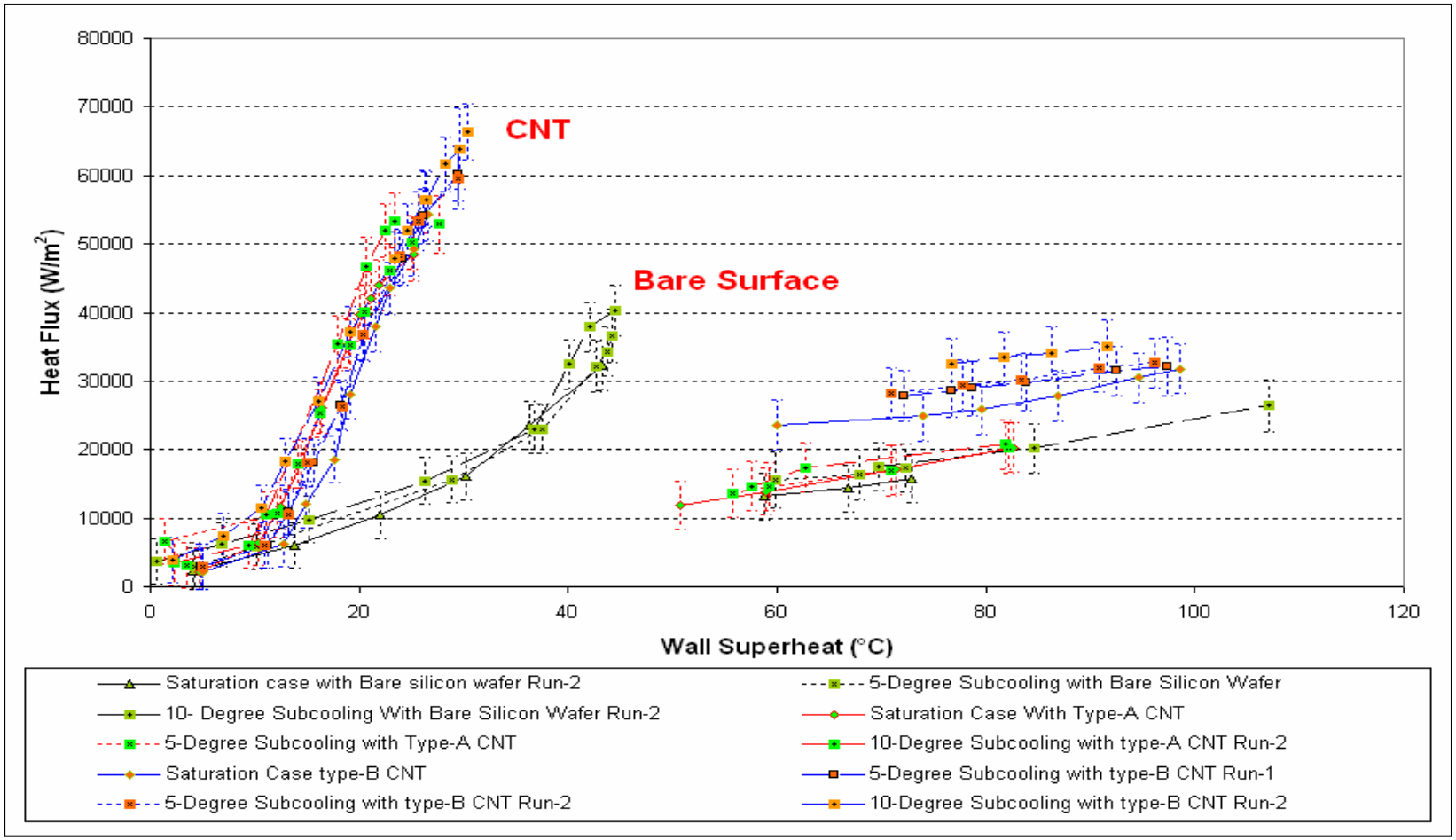

Fig. 8. Boiling curves for pool boiling of PF – 5060 at saturation and low subcooling conditions on the three test surfaces with error estimates. (Mr. Hee Seok Ahn's help in setting up the apparatus and acquisition of data in some of the low subcooling experiments is acknowledged and greatly appreciated. The saturation and 10-degree subcooling data for type-A CNT as well as the saturation data for type-B CNT has been reproduced from [46]).

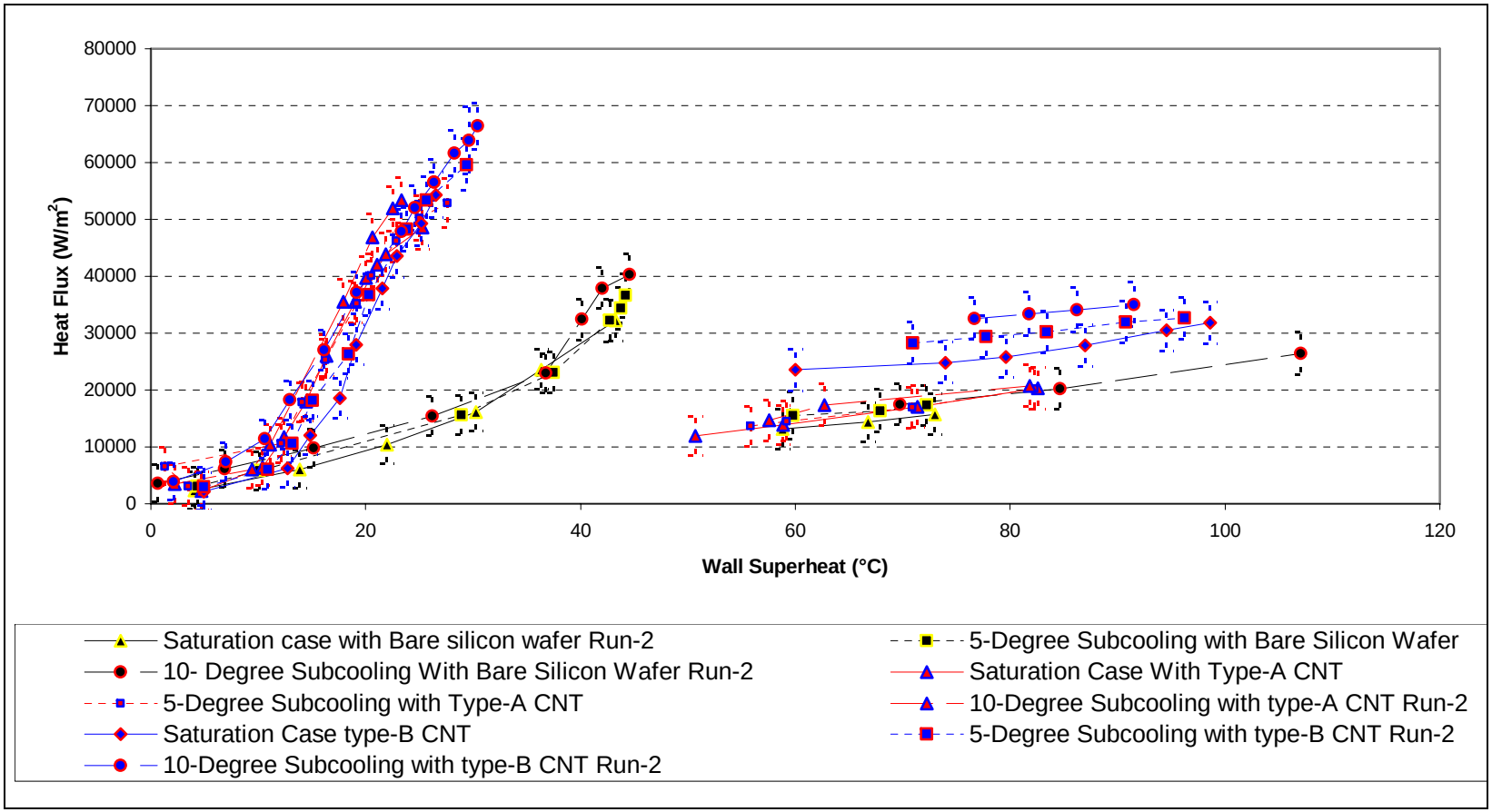

Fig. 9. Boiling curves at saturation and low subcooling conditions for pool boiling of PF- 5060 on three test surfaces for second set of runs. (Mr. Hee Seok Ahn's help in setting up the apparatus and acquisition of data in some of the low subcooling experiments is acknowledged and greatly appreciated. The saturation and 10-degree subcooling data for type-A CNT as well as the saturation data for type-B CNT has been reproduced from [46]).

b) *High Subcooling Cases:* Fig. 10 summarizes the results from the pool boiling experiments at high levels of subcooling of 20 and 30 °C. For the sake of clarity, Fig. 11 depicts the results from individual experimental runs for each subcooling, for the three surfaces.

It is seen that the surface with Type- A carbon nanotube shows a significant enhancement in boiling heat transfer over the bare silicon wafer in the nucleate boiling regime. However, presence of Type – A CNT seems to result in a marginal heat transfer enhancement in the film boiling regime. The overlap of the experimental uncertainties (Fig. 11) of Type-A CNT and that of the bare silicon wafer case in the film boiling regime precludes one from claiming an enhancement in heat transfer.

Fig. 12 shows the pool boiling curve for Type – B CNT at low and high subcooling. Type-B carbon nanotube shows a heat transfer enhancement over the corresponding bare silicon wafer case as well. However, the magnitude of increase in heat transfer is lower than that observed with Type-A CNT.

In these experiments (Fig. 12), the CHF condition could not be obtained at a subcooling level of 30 °C due to the limited capacity of the heat exchanger coil for sustaining the required level of subcooling.

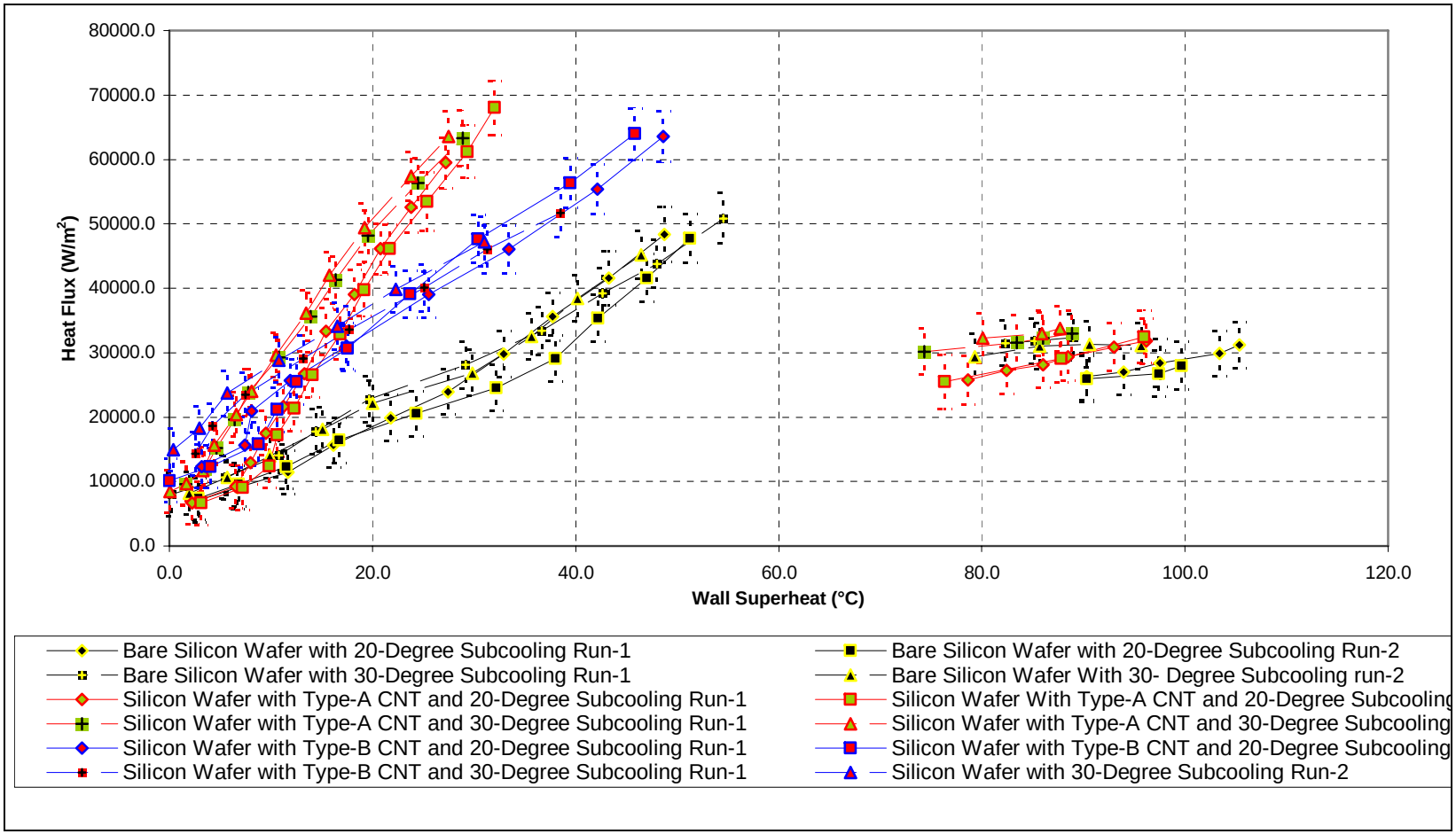

Fig. 10. Boiling curves for highly subcooled pool boiling experiments at subcooling levels of 20 °C and 30 °C for two test runs.

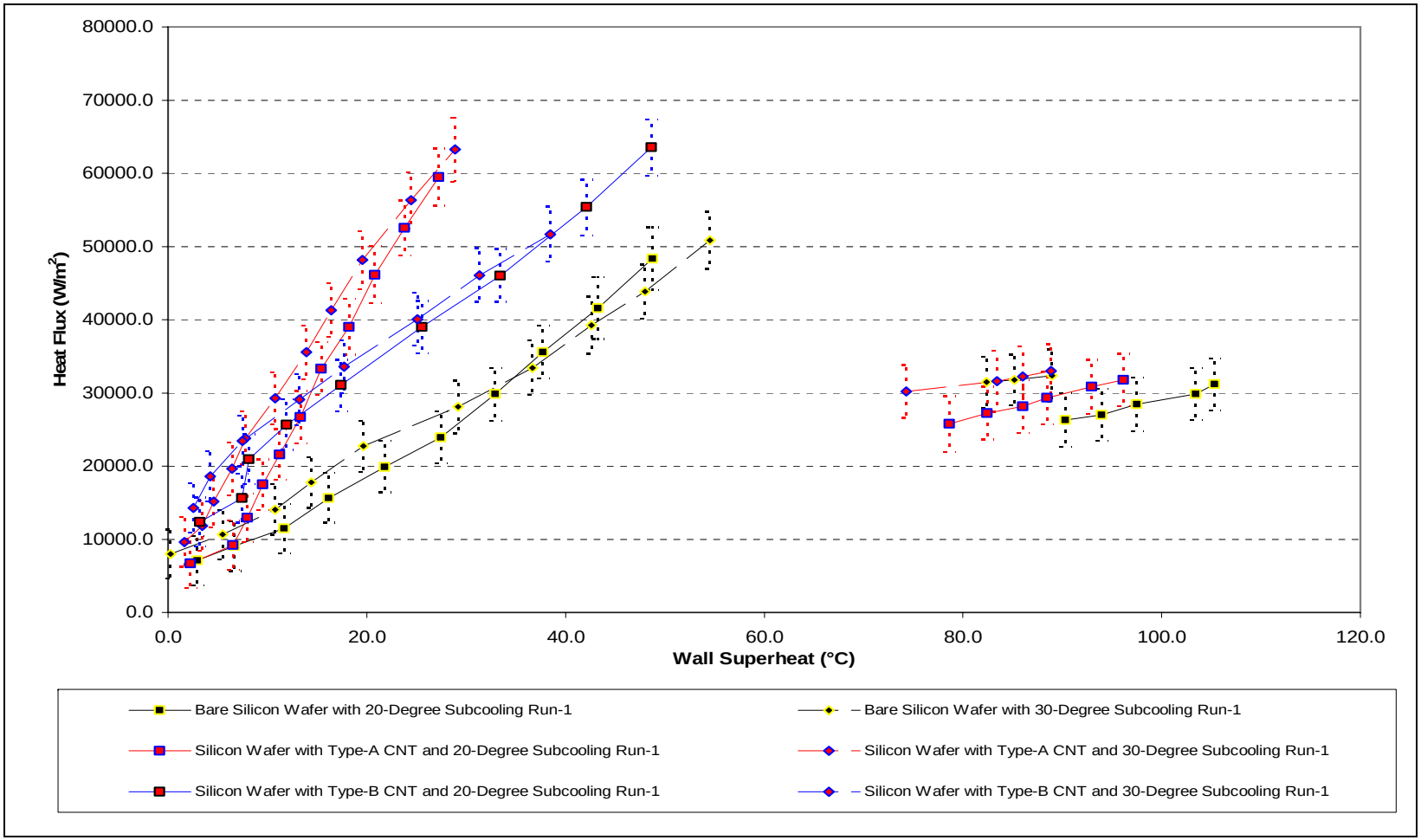

Fig. 11. Figure depicts pool the boiling curves of PF – 5060 at high subcooling levels of 20 °C and 30 °C on three different surfaces for a single test run.

In all cases a consistent trend was observed vis-à-vis the CHF point. The heat flux sustained close to CHF condition is significantly higher in case of test surfaces coated with CNT.

An anomalous trend is observed with the Type – B CNT for high subcooling. Four test runs were carried with this test surface, at a subcooling level of 30 °C and two for the 20 °C subcooling level in order to ensure repeatability and reliability of the data. For purposes of comparison, test data for low levels of subcooling has been reproduced (Figs. 12, 13 and 14) with the high subcooling test data superimposed. The inconsistency in the trend shown by the surface with Type- B CNT is seen clearly. There seems to be an apparent decrease in the performance (vis-à-vis the heat transfer) of the test surface at wall superheats in excess of 30 °C at subcooling levels of 20 and 30 °C as compared to the same surface in saturation, 5 °C subcooled, and 10 °C subcooled conditions.

Although the CHF under steady state conditions could not be obtained for the 30°C subcooling, it was found to occur at a significantly higher wall superheat as shown by the voltage setting required for causing onset of transition. This, tendency of the CHF to shift towards higher wall superheats are partly expected due to the significant disruption of the vapor film by the CNT. However, the Type-B CNT shows a decrease in performance at higher subcooling

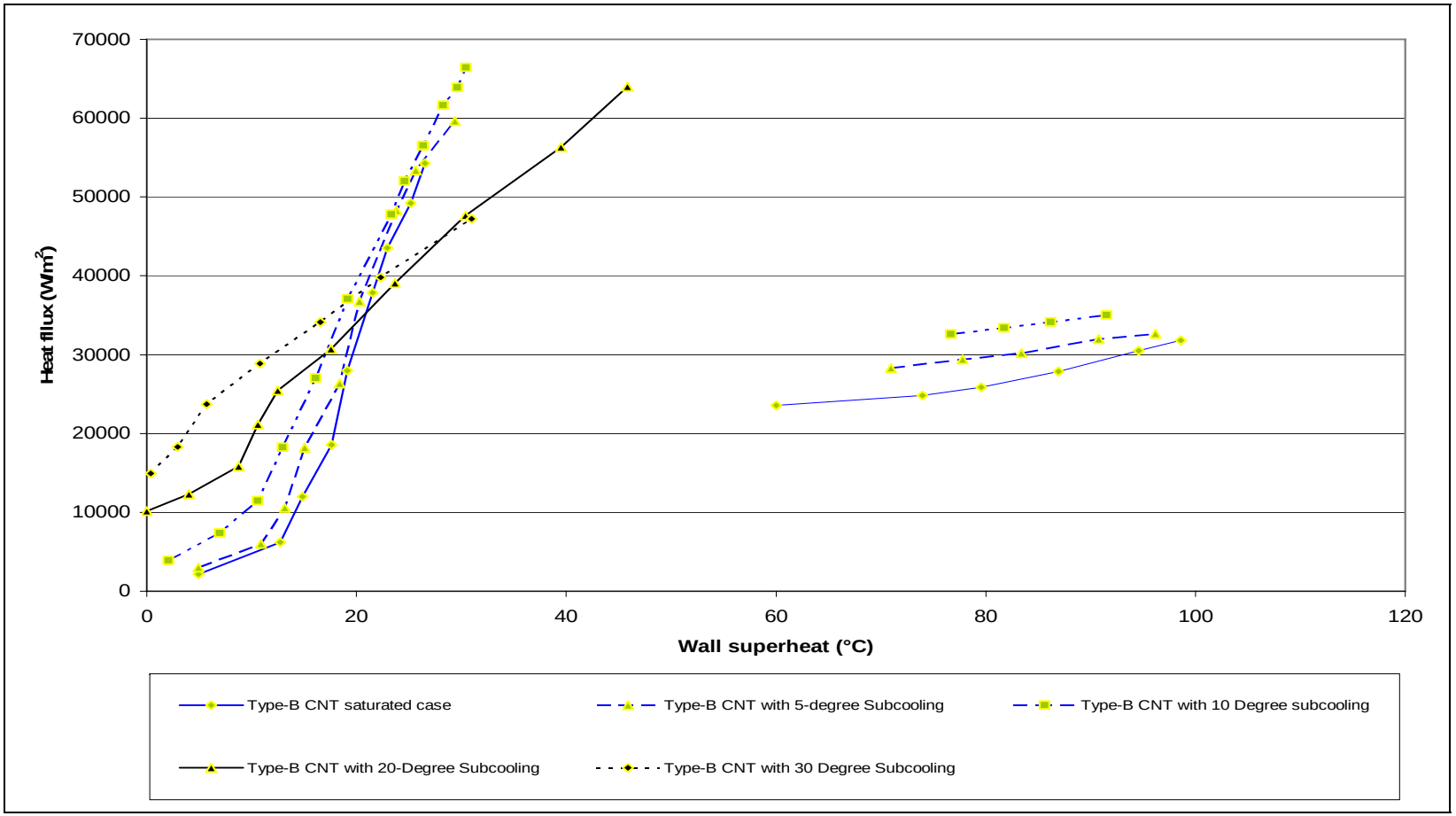

Fig. 12. Pool boiling curves of PF - 5060 on a test surface with Type-B CNT for various liquid pool temperatures. (Mr. Hee Seok Ahn's help in setting up the apparatus and acquisition of data in some of the low subcooling experiments is acknowledged and greatly appreciated. The saturation data for type-B CNT has been reproduced from [46]).

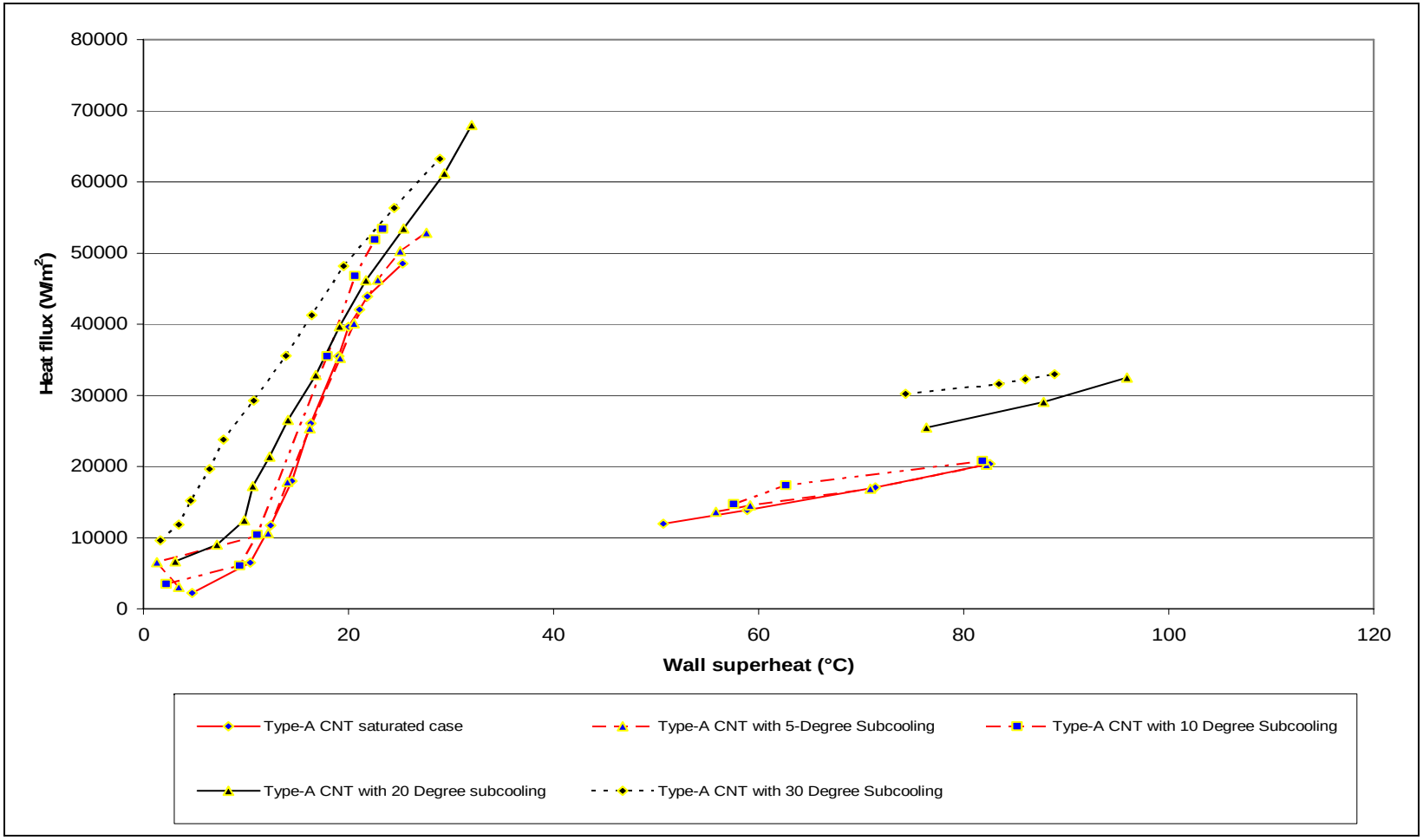

Fig. 13. Pool boiling curves of PF – 5060 on a test surface with Type –A CNT and various bulk liquid temperatures. (Mr. Hee Seok Ahn's help in setting up the apparatus and acquisition of data in some of the low subcooling experiments is acknowledged and greatly appreciated. The saturation and 10-degree subcooling data for type-A CNT has been reproduced from [46]).

levels as compared to the lower subcooling and saturation levels in the nucleate boiling regime. In these experiments, pool boiling curves for all four tests at 30 °C subcooling and for the two tests at 20 °C were found to be repeatable and consistent.

Figs. 13 and 14 depict the pool boiling curves for the test surfaces with Type-A MWCNT and bare silicon wafer respectively with varying bulk liquid temperatures. The data follows more consistent trends. The effect of subcooling is not very significant in the nucleate boiling regime. Subcooling enhances the heat transfer close to the CHF and shifts the CHF point towards higher wall superheats. The effects of subcooling are more perceptible in the film boiling regime. Furthermore, increase in subcooling tends to shift the Leidenfrost points towards higher wall superheats.

Tables A-1 through A-6 in Appendix - A show the calculated data for various test surfaces under highly subcooled conditions, subject to different levels of subcooling. The heat flux is observed to increase with increasing wall superheat until the CHF is obtained after which a dramatic decrease in the heat flux is observed as a result of the formation of a vapor film over the test surface. The absolute uncertainty is observed to remain approximately constant in magnitude with increase in wall superheat. Tables A-2 through A-6

show the test data for various test conditions. Similar trends are observed for all the cases.

Table A-7 summarizes the performance enhancement in heat transfer provided by the nano-textured surfaces as compared with the bare silicon wafer at the same subcooling level and a similar wall superheat.

Close to the CHF Type – A CNT leads to about 24 – 40% enhancement in heat transfer for a subcooling of 30 °C and about the same enhancement at a subcooling of 20 °C. In the nucleate boiling regime these values are about 75% for Type – A CNT with 20 °C subcooling and about 130% for a subcooling of 30 °C. Type - B CNT shows an enhancement of about 108 – 120% in the nucleate boiling regime for 20 °C subcooling. For a subcooling of 30 °C subcooling, Type – B CNT shows an enhancement of 85 – 90% in the nucleate boiling regime. The point with the maximum heat flux for Type - B CNT shows an enhancement of about 33% in the nucleate boiling regime for a subcooling of 20 °C.

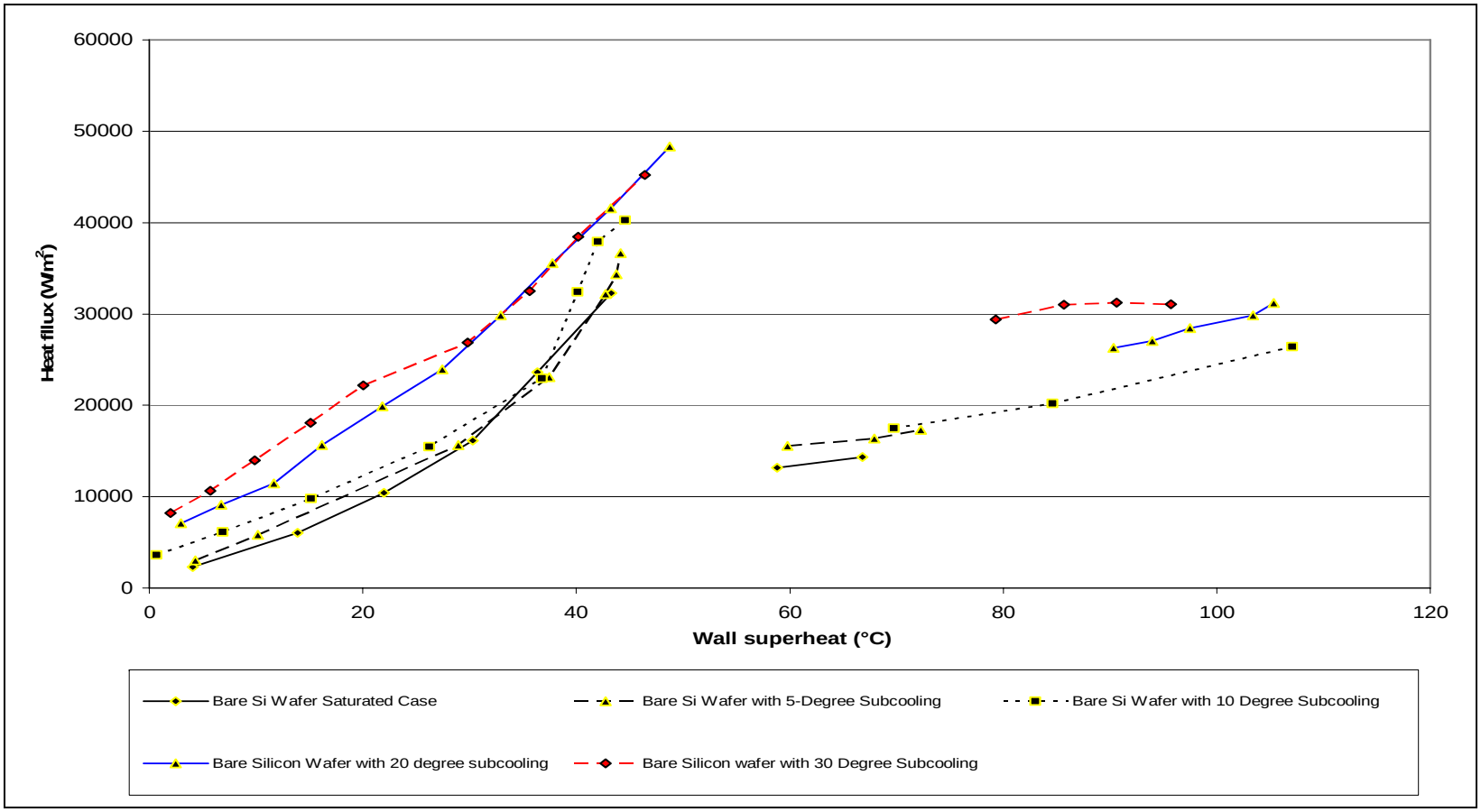

Fig. 14. Pool boiling curves of PF – 5060 on a bare silicon wafer and various bulk liquid temperatures. (Mr. Hee Seok Ahn's help in setting up the apparatus and acquisition of data in some of the low subcooling experiments is acknowledged and greatly appreciated.).

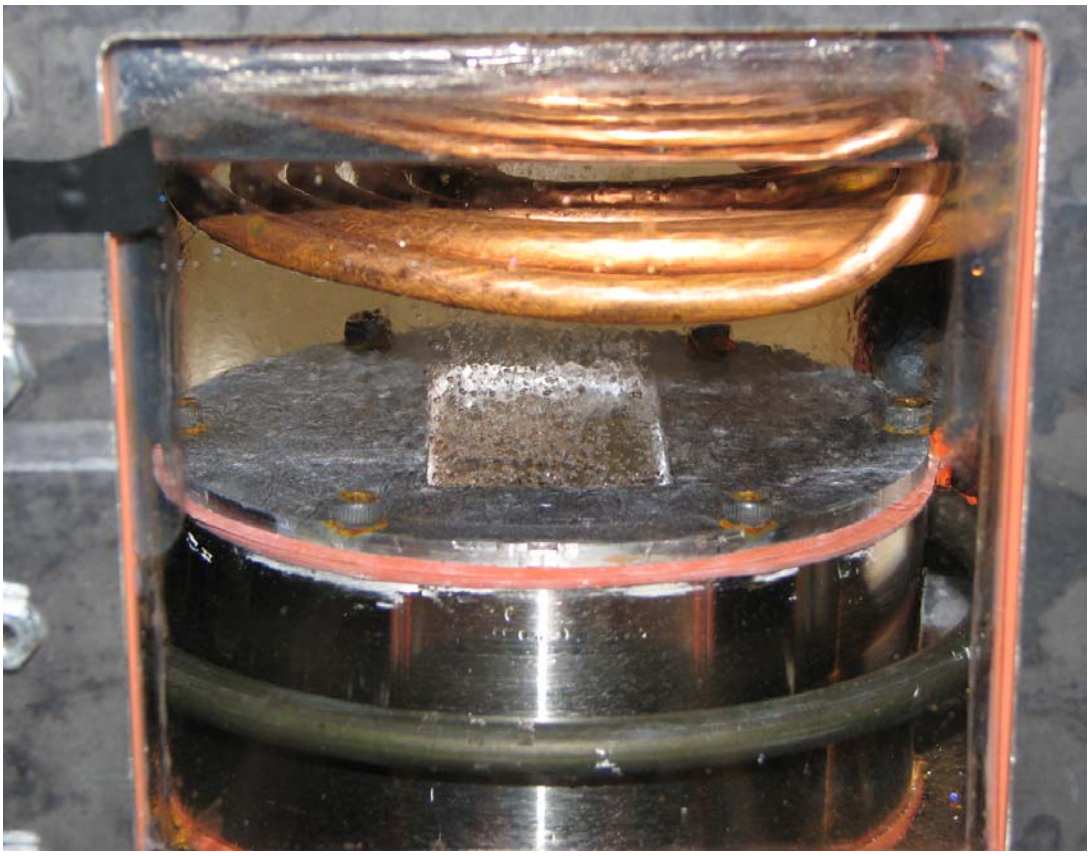

Fig. 15 Pool boiling on a bare silicon wafer at 30 °C subcooling close to CHF condition.

Figs. 15 and 16 depict the digital images acquired during the test, close to the CHF point for 30 °C subcooling on a bare silicon wafer and a wafer coated with Type-A CNT respectively. A large number of bubbles is seen to depart from the surface of the wafer with Type – A CNT than from the surface of the bare silicon wafer. This shows that the number of nucleation sites is much more in the latter case thus resulting in a significant heat transfer enhancement.

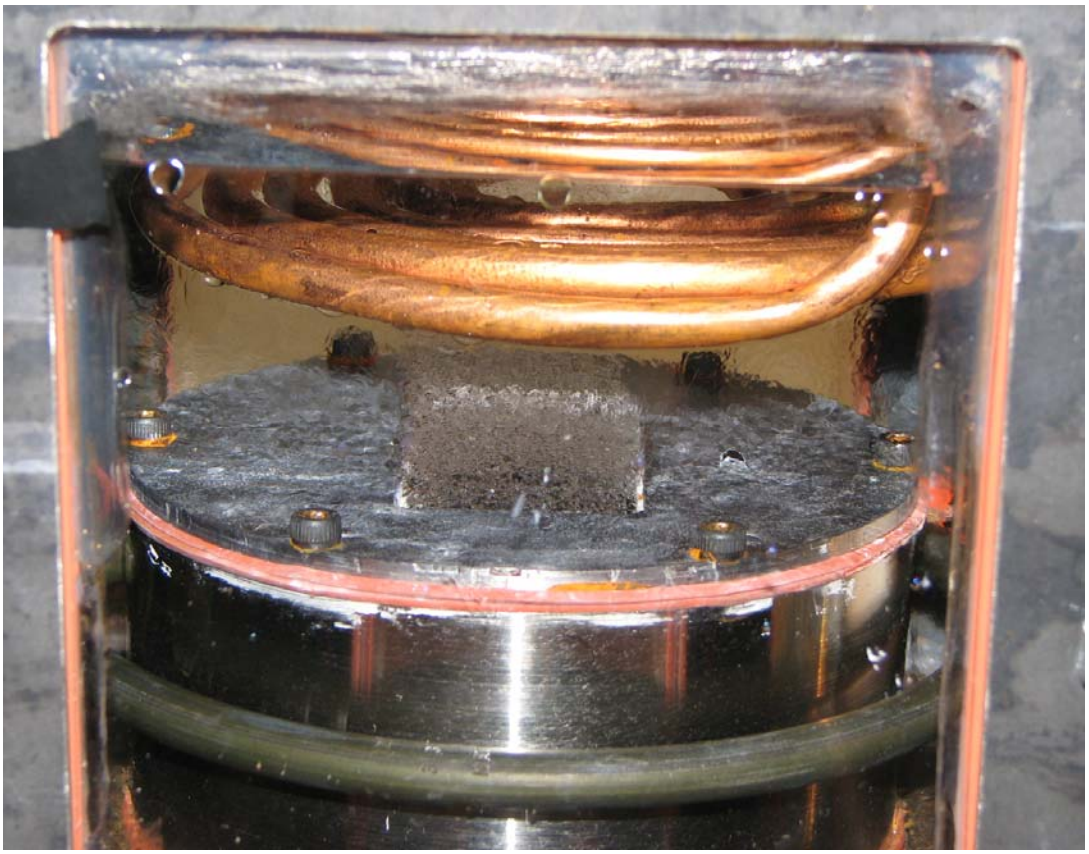

Fig. 16. Digital image of pool boiling near the CHF condition occurring at a subcooling level of 30 °C on a silicon wafer with Type-A CNT.

e) *Non-Departing Bubble Condition:* In addition to the above mentioned cases, a static bubble configuration was obtained at high liquid subcooling (~40 °C). A special heat exchanger coil was fabricated for this purpose using copper tubing with a quarter inch diameter. The coiled length of this heat exchanger is approximately 8 feet and is obtained by bending the coil at multiple levels.

In order to sustain subcooling levels greater than 30 °C, PF – 5060 is degassed and then chilled in a salted ice bath. After this the copper block is heated to approximately 200 °C and the constant temperature bath set to about -5 °C. The chilled PF – 5060 is then poured into the viewing chamber. This results in immediate film formation. Since the heat transfer rates to the liquid from the test surface is lower in the film boiling regime, the subcooling level can be sustained to achieve steady state conditions.

This condition is attained for the bare silicon wafer (with circular clamp, ~ 38 °C subcooling level, Ref. Table A-8, Appendix) and silicon wafer with Type – A CNT (rectangular clamp, ~ 33 °C, subcooling level). The non – departing condition is not attempted for the test surface with Type – B CNT. This is because; the film formation is expected to stabilize at temperatures of approximately 275 °C (for Type – B CNT) which exceeds the safe operating temperature of the test setup (~250 °C).

Figures, 18 and 20 depict the non – departing bubble condition on a silicon wafer and a silicon substrate coated with Type – A CNT. Recorded movie files show the merger and consequent departure of bubbles due to natural convection currents. The bubbles move around the surface and then tend to converge near the center,

merge and then depart from the surface. This is consistent with observations in the literature by Banerjee et al. [56-59].

Fig. 17 depicts film boiling on a bare silicon wafer at a subcooling level of 30 °C. Fig. 18 shows a digital image for the static or non - departing bubble condition on a circular bare silicon wafer at a subcooling of about 38 °C.

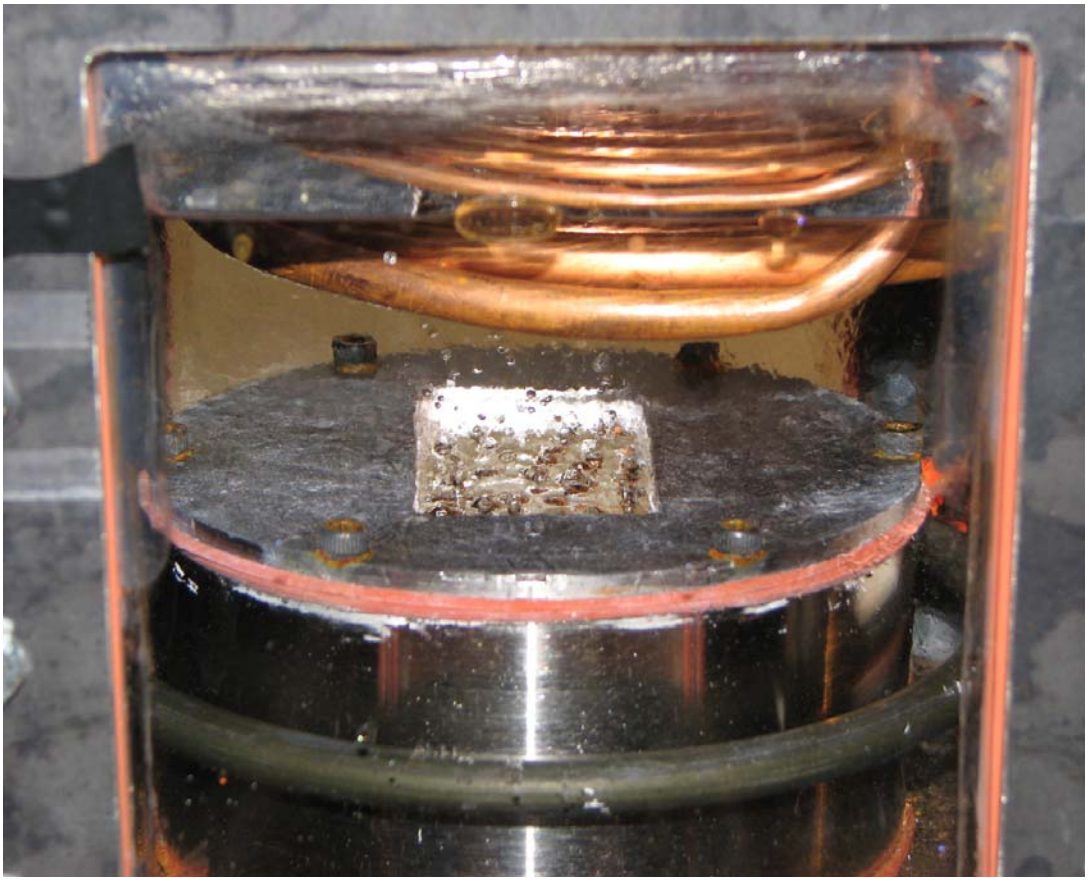

Fig. 17. The digital image depicts film boiling on a bare silicon wafer at a subcooling level of 30 °C.

A significant difference in the number of bubbles leaving the test surface is observed between the two images. Additionally, a relatively flat film is observed between adjacent bubbles in Fig. 18. In contrast, the film appears to be highly distorted in Fig. 17.

Fig. 18. Figure shows the non-departing bubble condition on a silicon wafer at ~ 37 °C subcooling level.

Fig. 19 shows the digital image of film boiling occurring at a subcooling level of 30 °C on silicon wafer with Type – A CNT. Fig. 20 depicts the static bubble configuration on a test surface with Type – A CNT. Again, a few large bubbles are seen leaving from the central region of the wafer due to bubble merger. The surface of the vapor film is relatively flat in Fig. 20 in contrast to the distorted film observed in Fig. 19.

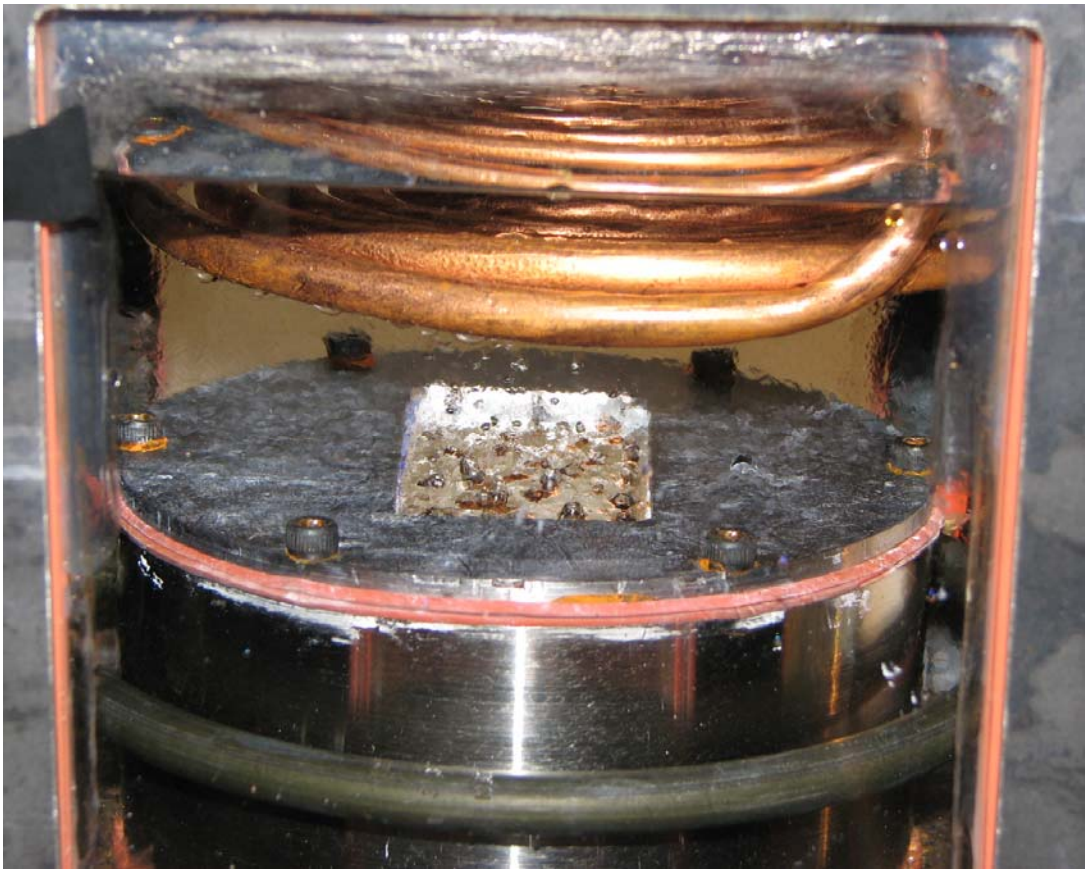

Fig. 19. Film boiling occurring at a subcooling level of 30 °C on a wafer coated with Type-A CNT.

Banerjee, ref. [56], observed the non-departing bubbles to be arranged in concentric rings on a circular heater. A similar configuration is observed in Fig. 18 above. Furthermore, mergers between contiguous bubbles on the same ring as well as merger of bubbles located on different rings were also observed in that study ([56]). The bubble mergers result in increased bubble volumes. The increased buoyancy force overcomes the surface tension and drag forces resulting in the formation of a "neck" and subsequent "pinch off" of the bubble.

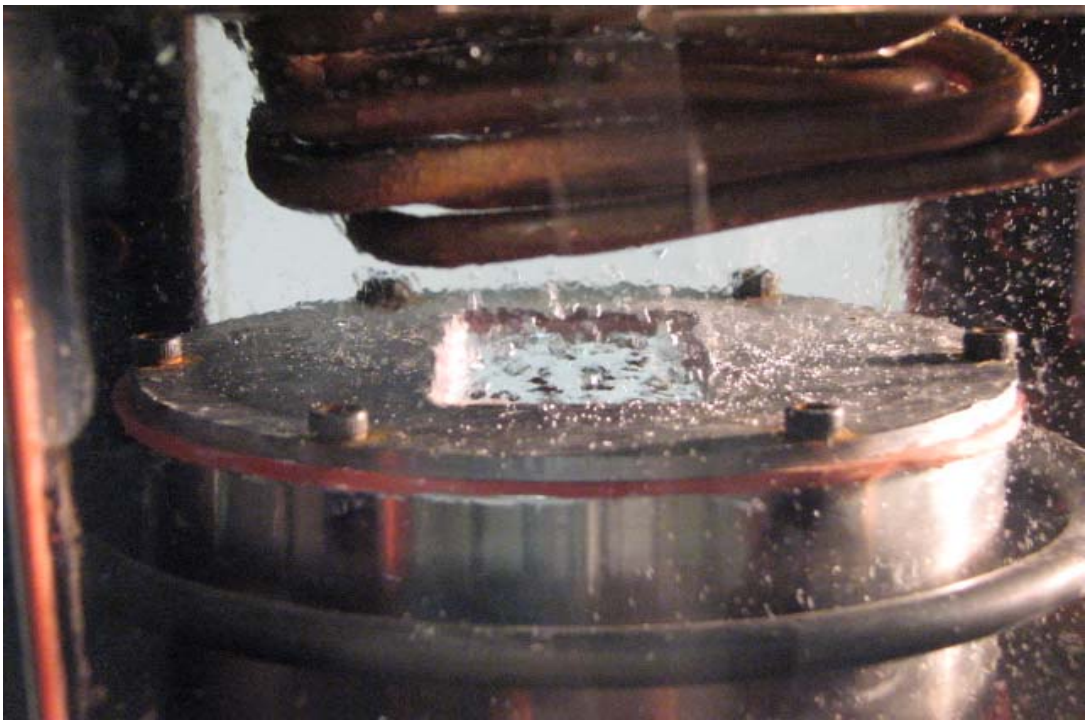

Fig. 20. Non – departing bubble configuration on a silicon wafer coated with Type – A CNT and with a rectangular cross section area for the second experimental run.

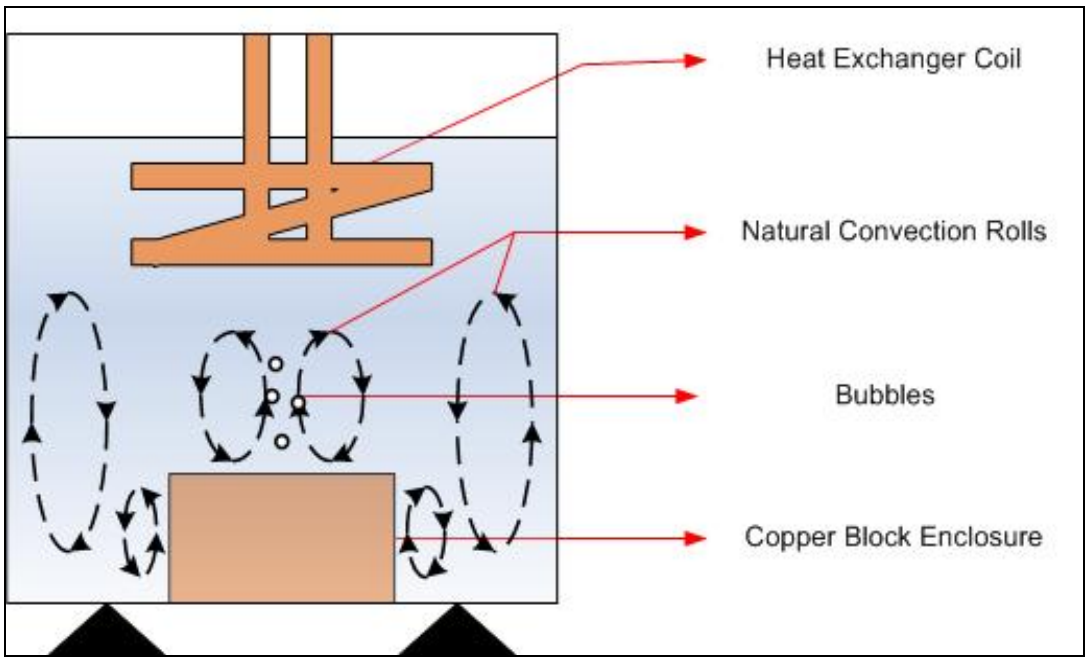

Fig. 21. Bubble motion caused by natural convection currents in the non – departing bubble condition.

Fig. 21 shows the schematic side view of the motion of the bubbles occurring in the non-departing bubble condition as a result of natural convection currents. Colder PF – 5060, in proximity to the cooling coils moves downwards whilst hotter PF-5060 from the heater surface rises up. This results in the formation of convection rolls on the heater surface which have a toroidal shape and were observed by Banerjee [56], using particle tracking velocimetry. The convective currents lead to radially inward motion of the test liquid

in close proximity to the liquid – vapor interface on the heater which results in a shear drag on the vapor bubbles. As a consequence, bubbles tend to move towards the center of the test surface. This liquid motion is also responsible for lateral merger of the vapor bubbles, causing bubble departure.

CHAPTER IV

SUMMARY AND CONCLUSION

4.1 Summary of Results

The experimental results from this study can be summarized as follows:

a) Pool boiling experiments were performed for PF-5060 on three different heater surfaces: bare silicon wafer, wafer coated with Type-A MWCNT (9 microns height) and Type-B MWCNT (25 microns height).

b) The experiments were conducted for saturated liquid, as well as for low liquid subcooling (5 ºC and 10 ºC) and high subcooling (20 ºC, 30 ºC and ~ 40 ºC for non-departing bubble configuration).

c) For saturated liquid and for low liquid subcooling experiments it was observed that the presence of the MWCNT enhanced nucleate boiling heat flux, irrespective of the size of the MWCNT.

d) For high liquid subcooling, Type-B MWCNT displayed anomalous behavior.

e) For film boiling condition, heat flux was not enhanced by Type-A MWCNT while Type-B MWCNT enhanced heat flux by considerable margins.

f) In the film boiling regime, the enhancement in heat flux decreased for Type-B MWCNT than for saturated film boiling when compared to the bare silicon wafer surface.

g) Images were acquired during the steady pool boiling conditions in the vicinity of the Critical Heat Flux (CHF) condition and the Leidenfrost condition as well as the non-departing bubble configuration at high subcooling. It was observed that more bubbles nucleated and departed from the heated surface at CHF in the presence of the MWCNT (irrespective of the height of the MWCNT). In the film boiling regime similar number of bubbles were found to form and depart from Type-A MWCNT and bare silicon wafer for low values of liquid subcooling. At high values of liquid subcooling (non-departing bubble configuration) it was observed that the vapor film was markedly distorted for the Type-A MWCNT compared to the vapor film observed on bare silicon wafer.

4.2 Possible Mechanisms for Heat Transfer Enhancement

The experimental results were used to identify the potential mechanisms responsible for the observed enhancement in pool boiling heat transfer on MWCNT coated surfaces compared to the bare surface:

a) *Disruption of Microlayer:* In nucleate boiling, the CNT tends to disrupt the "microlayer" under the bubbles leading to enhanced heat transfer.

b) *Increased Number of Active Nucleation Sites:* As observed in the digital images, the number of nucleation sites in case of the wafer coated with CNT seems to be higher than that of a bare silicon wafer. This could be responsible for the significant enhancement in the heat transfer for nucleate pool boiling.

c) *High Thermal Conductivity of Nanotubes and the Nano-fin Effect:* The high thermal conductivity of CNT and the consequent nano-fin effect could be another factor. The CNT potentially behave as a enhanced heat transfer surface and could lead to a lower temperature differential between the surface of the substrate and the tips of the CNT resulting in very efficient heat transfer to the test fluid.

d) *Enlargement in Size of Cold Spots:* Additionally "cold spots" Ref. [46], formed on a boiling surface can be enhanced by MWCNT. Cold spots form due to coupled non-linear thermal and hydro-dynamic interactions which cause spatio-temporal re-distribution of the wall temperature. This causes the cold spots to serve as focused conduits for the surface heat flux distribution. The size of the cold spots is predicted to be proportional to the heater material properties [57 – 59] (e.g., thermal conductivity or diffusivity). MWCNT have higher thermal conductivity as well as thermal diffusivity and therefore potentially enlarged the size of the cold spots that formed

on the boiling surface. This could lead to enhancement of the total heat flux in boiling.

e) *Transient Liquid–Solid Contact:* Coupled with the enhancement in cold spot size, the disruption of the vapor film in film boiling (surface with Type – B CNT) and the consequent transient liquid-solid contact could be playing a role in heat transfer enhancement in film boiling.

f) *Pinning of the Contact Line:* Pinning of the liquid-vapor interface on the heater due to presence of the MWCNT could enhance the surface area for latent heat transfer under individual bubbles. This could also be a potential mechanism for enhanced pool boiling heat transfer on MWCNT.

4.3 Future Directions

The experimental results from this study point to a number of mechanisms responsible for enhancement of the pool boiling heat transfer observed on nano-textured surfaces. The relative proportion and the relative contribution to the total heat flux by the different mechanisms are not apparent from these results. Following issues can be identified for future studies on pool boiling heat flux on nano-structured surfaces:

(a) Experiments and numerical models can be devised to explore the relative contribution of the different mechanisms to the total heat flux. The next step would be to identify and quantify the effect of

each of the aforementioned factors on the heat transfer enhancement and identify the key contributors.

(b) The surface temperature in pool boiling on nano-structured surfaces need to be resolved by direct measurement (instead of the indirect metrology techniques employed in this study). Micro-fabricated temperature sensors (or temperature nano-sensors) can be integrated with the nano-structured surfaces for measuring the surface temperature during pool boiling experiments. The micro/nano-sensors need to be designed such that the sensing techniques cause minimal interference of the transport mechanisms.

(c) The non-linear coupled hydrodynamic and thermal interactions on nano-structured surfaces ("cold spots") could also be measured using these temperature micro/nano- sensors. Such temperature data can be analyzed using non-linear dynamic techniques ("chaos theory") for studying the change in the order of the non-linear complexity of the system (or degrees of freedom of the boiling system). The change in the order of complexity due to the presence of MWCNT can be explored in the different boiling regimes at various wall superheat and liquid subcooling. Such temperature transients ("cold spots") are predicted to demonstrate cooling capacities of ~1MW/cm^2 on conventional surfaces and are expected to be of higher magnitude on properly designed nano-structured surfaces. If these temperature

transients can be harnessed by appropriately designed boiling surfaces it can lead to development of heat exchanger devices with unprecedented levels of cooling capacity.

REFERENCES

[1] J. G. Leidenfrost, De Aquae Communis Nonnullis Qualitatibus Tractatus, (A Tract about Some Qualities of Common Water), Duisburg, 1756; The Pertinent Portions are Reprinted in Translation in Int. J. Heat Mass Transfer 9 (1966) 1153-1166.

[2] S. Nukiyama, The Maximum and Minimum Values of the Heat Q Transmitted from Metal to Boiling Water under Atmospheric Pressure, Journal of Japan Society of Mechanical Engineers 37 (1934) 367-374; Reprinted in International Journal of Heat and Mass Transfer 27 (7) (1984) 959- 970.

[3] J.W. Westwater, J.G. Santangelo, Photographic Study of Boiling, Industrial and Engineering Chemistry, 47 (8) (1955) 1605 – 1610.

[4] Y.Y. Hsu, J.W. Westwater, Film Boiling from Vertical Tubes, A.I.Ch.E. Journal 54 (1) (1958) 58 – 62.

[5] Rayleigh, On the Pressure Developed in a Liquid during the Collapse of a Spherical Cavity, Phil. Mag. 34 (1917) 94-98.

[6] M. Jakob, W. Fritz, Versuche über den Verdampfungsvorgang, Forsch. Geb. Ingenieurwes., 2 (1931) 435-447.

[7] M. Jakob, W. Linke, Der Wa¨rmeu¨bergang von einer. waagerechten Platte an siedendes Wasser, Forsch. Geb. Ing. 4 (1933) 75-81.

[8] I.L. Pioro, W. Rosenhow, S.S. Doerffer, Nucleate Pool-Boiling Heat Transfer. I: Review of Parametric Effects of Boiling Surface, International Journal of Heat and Mass Transfer 47 (2004) 5033-5044.

[9] C. Ramaswamy, Y. Joshi, W. Nakayama, W.B. Johnson, Effects of Varying Geometrical Parameters on Boiling from Microfabricated Enhanced Structures, Journal of Heat Transfer 125 (2003) 103 – 109.

[10] J. Coursey, J. Kim, H. Roh, P. J. Boudreaux, Graphite Foam Thermosyphon Evaporator Performance: Parametric Investigation of the Effects of the Working Fluid, Liquid Level, and Chamber Pressure, Proceedings of ASME IMECE-2002, IMECE-2002-33733, New Orleans, Louisiana, November 17-22, 2002, 1-6.

[11] O.S. Ujereh, I. Mudawar, P.B. Amama, T.S. Fisher, W. Ou, Enhanced Pool Boiling on Carbon Nanotube Arrays on a Silicon Surface, Proceedings of ASME IMECE-2005, IMECE2005-80065, Orlando, Florida, November 5-11, 2005, 1-6.

[12] A. Oberline, M. Endo, T. Koyama, High Resolution Electron Microscope Observations of Graphitized Carbon Fibers, Carbon 14 (1976) 133-135.

[13] A. Oberline, M. Endo, T. Koyama, Filamentous Growth of Carbon through Benzene Decomposition, Journal of Crystal Growth 32 (1976) 335-349.

[14] M. Endo, A. Oberlin, T. Koyama, High Resolution Electron Microscopy of Graphitizable Carbon Fiber Prepared by Benzene Decomposition, Japanese Journal of Applied Physics 16 (9) (1977) 1519-1523.

[15] S. Iijima, Helical Microtubules of Graphitic Carbon, Letters to Nature 354 (1991) 56-58.

[16] M.P. Anantram, F. Léonard, Physics of Carbon Nanotube Devices, Reports on Progress in Physics, Institute of Physics Publishing 69 (2006) 507 – 561.

[17] J.-P. Salvetat, J.-M. Bonard, N.H. Thomson, A.J. Kulik, Forró, W. Benoit, L. Zuppiroli, Mechanical Properties of Carbon Nanotubes, Applied Physics A, Materials Science and Processing 69 (1999) 255 – 260.

[18] H. Dai, N. Franklin, J. Han, Exploiting Properties of Carbon Nanotubes for Nanolithography, Applied Physics Letters 73 (11) (1998) 1508 – 1510.

[19] M. Terrones, Science and Technology of the Twenty-First Century: Synthesis, Properties, and Applications of Carbon Nanotubes, Annual Review of Material Research 33 (2003) 419 – 501.

[20] M.S. Dresselhaus, P.C. Eklund, Phonons in Carbon Nanotubes, Advances in Physics 49 (6) (2000) 705 – 814.

[21] J. Hone, M. Whitney, C. Piskoti, A. Zettl, Thermal Conductivity of Single-Walled Carbon Nanotubes, Rapid Communications, Physics Review B 59 (1999) 2514-2516.

[22] J. Che, T. Çağin, W. A. Goddard, Thermal Conductivity of Carbon Nanotubes, Nanotechnology 11 (2000) 65-69.

[23] S. Berber, Y-K. Kwon, D. Tománek, Unusually High Thermal Conductivity of Carbon Nanotubes, Physical Review Letters 84 (20) (2000) 4613-4619.

[24] P.Kim, L.Shi, A.Majumdar and P.L. McEuen, Thermal Transport Measurements of Individual Multiwalled Nanotubes, Physical Review Letters 87 (21) (2001) 215502-1 – 215502-4.

[25] D. Wen, Y. Ding, Effective Thermal Conductivity of Aqueous Suspensions of Carbon Nanotubes (Carbon Nanotube Nanofluids), Journal of Thermophysics and Heat Transfer 18 (4) (2004) 481-485.

[26] S.U.S. Choi, Enhancing Thermal Conductivity of Fluids with Nanoparticles, Developments and Applications of Non-Newtonian Flows, ASME FED231/MD66 (1995), pp. 99-103.

[27] P. Keblinski, S.R. Phillpot, S.U.S. Choi, J.A. Eastman, Mechanisms of Heat Flow in Suspensions of Nano-Sized Particles (Nanofluids), International Journal of Heat and Mass Transfer 45 (4) (2002) 855 – 863.

[28] S. Lee, S.U.S. Choi, S. Li, J.A. Eastman, Measuring Thermal Conductivity of Fluids Containing Oxide Nanoparticles, Journal of Heat Transfer 121 (2) (1999) 280 -289.

[29] Y. Xuan, Q. Li, Investigation on Convective Heat Transfer and Flow Features of Nanofluids, Journal of Heat Transfer 125 (2003) 151 – 155.

[30] Y. M. Xuan, W. Roetzel, Conceptions for Heat Transfer Correlations of Nanofluids, International Journal of Heat and Mass Transfer 43 (19) (2000) 3701 – 3707.

[31] J.A. Eastman, S.R. Philpot, S.U.S. Choi, P. Keblinski, Thermal Transport in Nanofluids, Annual Review of Materials Research 34 (2004) 219 – 246.

[32] H. Masuda, A. Ebata, K. Teramae, and N. Hishinuma, Netsu Bussei 4 (1993) 227-233.

[33] S. Lee, S.U.S. Choi, S. Li, J.A. Eastman, Measuring Thermal Conductivity of Fluids Containing Oxide Nanoparticles, Journal of Heat Transfer 121 (2) (1999) 280 – 289.

[34] H. Xie, J. Wang, T. Xi, Y. Liu, F. Ai, Q. Wu, Thermal Conductivity Enhancement of Suspensions Containing Nanosized Alumina Particles, Journal of Applied Physics 91 (7) 4568 – 4572.

[35] H. Xie, J. Wang, T. Xi, Y. Liu, Thermal Conductivity of Suspensions Containing Nanosized SiC Particles, International Journal of Thermophysics 23 (2) (2002) 4568 - 4572.

[36] L.P. Zhou, B.X. Wang, Experimental Research on the Thermophysical Properties of Nanoparticle Suspensions Using the Quasi-steady State Method, Annual Proceedings Chinese Eng. Thermophysics, Shanghai 2002, 889 – 892.

[37] J.A. Eastman, S.U.S. Choi, S. Li, W. Yu, L.J. Thompson, Anomalously Increased Effective Thermal Conductivity of Ethylene Glycol Based Nanofluids Containing Copper Nanoparticles, Applied Physics Letters 78 (6) (2000) 718 – 720.

[38] S.K. Das, N. Putra, W. Roetzel, Pool Boiling Characteristics of Nanofluids, International Journal of Heat and Mass Transfer 46 (2003) 851 – 862.

[39] S.M. You, J.H. Kim, K.H. Kim, Effect of Nanoparticles on Critical Heat Flux of Water in Pool Boiling Heat Transfer, Applied Physics Letters 83 (16) (2003) 3374 – 3376.

[40] P. Vasallo, R. Kumar, S. D' Amico, Pool Boiling Heat Transfer Experiments in Silica-water Nano-fluids, International Journal of Heat and Mass Transfer 47 (2004) 407 – 411.

[41] I. C. Bang, S. H. Chang, Direct Observation of a Liquid Film under a Vapor Environment in a Pool Boiling Using a Nanofluid, Applied Physics Letters, 86 (2005) 134107-1 – 134107-3.

[42] K. Sefiane, On the Role of Structural Disjoining Pressure and Contact Line Pinning in Critical Heat Flux Enhancement during Boiling of Nanofluids, Applied Physics Letters, 89 (2006) 044106-1 – 044106-3.

[43] I. Mudawar, Assessment of High Heat Flux Thermal Management Schemes, IEEE Transactions on Components and Packaging 124 (2) (2001) 122 – 141.

[44] M. Zhang, S. Fang, A.A. Zakhidov, S.B. Lee, A.E. Aliev, C.D. Williams, K.R. Atkinson, R. Baughman, Strong, Transparent, Multifunctional, Carbon Nanotube Sheets, Science 309 (2005) 1215-1219.

[45] H-S. Ahn, N. Sinha, M. Zhang, S. Fang, R. H. Baughman, D. Banerjee, Pool Boiling Experiments on Multi-Walled Carbon Nanotube (MWCNT) Forests, ASME Journal of Heat Transfer 128 (2006) (in print).

[46] H-S Ahn, V. Sathyamurthi, S. Lau, D. Banerjee, Boiling Experiments Using Vertically Aligned Carbon Nanotubes and Using Surface Micromachined

Thin-Film Thermocouples (TFT), AIAA 2006 – 2916, 9th Joint AIAA/ASME Thermophysics and Heat Transfer Conference, San Francisco, California, 5 – 8 Jun 2006, 1-10.

[47] N. Sinha, Design, Fabrication, Packaging and Testing of Thin Film Thermocouples for Boiling Studies, M.S. Thesis, Texas A&M University, College Station, 2006.

[48] Y.Y. Hsu, F.F. Simon, R.W. Graham, Application of Hotwire Anemometry for Two Phase Flow Measurements Such as Void Fraction and Slip, Proceedings of the ASME Winter Meeting, Philadelphia, PA, 1963, 26 -34.

[49] H. Toral, A Study of Hot – wire Anemometer for Measuring Void Fraction in Two Phase Flow, Journal of Physics E, Sci. Instrum. 14 (1981) 822 – 827.

[50] G.E. Dix, Vapor Void Fractions for Forced Convection with Subcooled Boiling at Low Flow Rates, Phd Dissertation, University of California, Berkeley, 1971.

[51] L.E. Gill, G.F. Hewitt, and J.W. Hitchton, Sampling Probe Studies of the Gas Core in Annular Two Phase Flow, Che. Eng. Sci. 18 (1963) 525 – 525.

[52] S. Chatpun, M. Watanabe, M. Shoji, Nucleation Site Interaction in Pool Nucleate Boiling on Heated Surface with Triple Artificial Cavities, International Journal of Heat and Mass Transfer 47 (2004) 3583 – 3587.

[53] G. Comte-Bellot, Hot-Wire Anemometry, Annual Reviews of Fluid Mechanics 8 (1976) 209 – 231.

[54] G.T.A. Kovacs, Chapter 6: Thermal Transducers, in Micromachined Transducers Sourcebook, WCB McGraw Hill, New York, 1998.

[55] S.J. Kline, F.A. Mc Clintock, Describing Uncertainties in Single – Sample Experiments, Mech. Eng. 75 (1953) 3 – 8.

[56] D. Banerjee, Numerical and Experimental Investigation of Subcooled Film Boiling on a Horizontal Plate, Ph. D. dissertation, University of California, Los Angeles, 1999.

[57] D. Banerjee, V.K. Dhir, Study of Subcooled Film Boiling on a Horizontal Disc: Part 1 Analysis, Journal of Heat Transfer 123 (2001) 271-284.

[58] D. Banerjee, V.K. Dhir, Study of Subcooled Film Boiling on a Horizontal Disc: Part 2 Experiments, Journal of Heat Transfer 123 (2001) 285-293.

[59] D. Banerjee, G. Son, V.K. Dhir, Conjugate Thermal and Hydrodynamic Analysis of Saturated Film Boiling from a Horizontal Surface, ASME HTD 334, Part 3 (1996) 57-64.

APPENDIX A

SELECTED EXPERIMENTAL RESULTS

Table A-1

Test data for Bare Silicon wafer with 20 °C subcooling.

Wall Superheat (°C)	Heat Flux (W/m^2)	Relative Uncertainty	Absolute Uncertainty (W/m^2)
3.0	7085.8	0.47	3358.83
6.7	9088.5	0.37	3377.59
11.7	11465.1	0.29	3368.80
16.2	15651.8	0.22	3435.07
21.8	19899.6	0.18	3517.95
27.4	23915.3	0.15	3530.83
32.9	29835.4	0.12	3597.58
37.7	35582.7	0.10	3642.99
43.2	41567.2	0.10	4214.52
48.7	48336.1	0.09	4257.34
90.3	26295.8	0.14	3626.84
94.0	27026.1	0.13	3543.44
97.5	28431.2	0.13	3695.86
103.4	29851.3	0.12	3507.44
105.4	31188.4	0.11	3569.18

Table A-2

Test data for Bare Silicon wafer with 30 °C subcooling.

Wall Superheat (°C)	Heat Flux (W/m^2)	Relative Uncertainty	Absolute Uncertainty (W/m^2)
0.2	8012.2	0.42	3369.44
5.5	10657.7	0.32	3390.41
10.8	14048.7	0.24	3434.16
14.4	17756.0	0.20	3474.70
19.7	22740.0	0.15	3514.75
29.2	28090.1	0.13	3621.98
36.7	33420.1	0.11	3718.05
42.6	39251.0	0.10	3912.53
48.0	43819.3	0.08	3715.43
54.5	50844.7	0.08	3934.30
82.4	31463.3	0.11	3518.35
85.2	31798.7	0.11	3492.54
89.0	32380.0	0.11	3556.39

Table A-3

Test data for test surface coated with Type-A MWCNT at 20 °C subcooling.

Wall Superheat (°C)	Heat Flux (W/m^2)	Relative Uncertainty	Absolute Uncertainty (W/m^2)
2.2	6686.5	0.50	3354.58
6.6	9188.9	0.37	3362.95
8.0	12920.6	0.26	3373.88
9.5	17479.5	0.20	3420.21
11.2	21585.4	0.16	3479.00
13.3	26698.3	0.13	3529.88
15.4	33323.0	0.11	3581.19
18.2	39030.5	0.10	3817.33
20.8	46134.7	0.09	3931.08
23.8	52543.0	0.07	3810.40
27.2	59494.7	0.07	3903.87
78.6	25752.9	0.15	3792.84
82.4	27251.1	0.13	3643.98
86.0	28160.2	0.13	3597.24
88.5	29330.2	0.12	3618.57
93.0	30817.5	0.12	3692.58
96.2	31794.4	0.11	3546.64

Table A-4

Test data for 30 °C subcooling with Type-A CNT.

Wall Superheat (°C)	Heat Flux (W/m^2)	Relative Uncertainty	Absolute Uncertainty (W/m^2)
1.6	9625.5	0.35	3375.29
3.5	11846.9	0.29	3424.06
4.6	15169.3	0.23	3515.33
6.4	19641.8	0.18	3613.55
7.8	23799.9	0.15	3635.42
10.8	29256.3	0.12	3598.82
13.9	35582.3	0.10	3659.63
16.4	41284.1	0.09	3654.63
19.5	48149.2	0.08	3980.92
24.5	56307.8	0.07	3855.60
28.9	63260.7	0.07	4378.94
74.3	30186.4	0.12	3566.64
83.4	31601.7	0.13	4181.31
86.0	32223.9	0.13	4108.55
88.9	32980.8	0.11	3631.13

Table A-5

Test data for 20 °C subcooling with Type-B CNT.

Wall Superheat (°C)	Heat Flux (W/m^2)	Relative Uncertainty	Absolute Uncertainty (W/m^2)
3.2	12348.5	0.27	3363.31
7.4	15610.2	0.22	3389.93
8.1	20909.5	0.16	3402.11
11.9	25647.0	0.13	3454.29
17.4	31062.7	0.11	3512.97
25.5	38996.6	0.09	3569.01
33.4	46029.8	0.08	3663.86
42.1	55379.5	0.07	3832.65
48.6	63533.5	0.06	3894.89

Table A-6

Test data for 30 °C subcooling with Type-B CNT.

Wall Superheat (°C)	Heat Flux (W/m^2)	Relative Uncertainty	Absolute Uncertainty (W/m^2)
2.6	14302.5	0.24	3366.89
4.2	18626.2	0.18	3406.79
7.5	23459.8	0.15	3430.83
13.2	29116.9	0.12	3491.07
17.7	33596.1	0.11	3564.93
25.1	40071.7	0.09	3637.88
31.3	46064.6	0.08	3696.66
38.5	51687.1	0.07	3748.86

Table A-7

Summary of heat transfer enhancements for 20 and 30 °C high subcooling cases.

Test Surface	Run	Subcooling Level (°C)	Wall Superheat (°C)	Heat Flux (W/m^2)	Percent Improvement (Min)	Percent Improvement (Max.)
Bare Silicon (Nucleate Boiling)	1	20	11.7	11465.1	-	-
	2	20	11.5	12330.2	-	-
Type-A CNT (Nucleate Boiling)	1	20	11.2	21585.4	75.06	88.27
	2	20	12.3	21384.7	73.43	86.52
Type-B CNT (Nucleate Boiling)	1	20	11.9	25647.0	108.00	123.70
	2	20	12.5	25477.1	106.62	122.22
Bare Silicon (CHF)	1	20	48.7	48336.1	-	-
	2	20	51.3	47761.1	-	-
Type-A CNT (CHF)	1	20	27.2	59494.7	23.09	24.57
	2	20	32.0	68005.3	40.69	42.39
Type-B CNT (CHF)	1	20	48.6	63533.5	31.44	33.02
	2	20	45.9	63978.7	32.36	33.96
Bare Silicon (Nucleate Boiling)	1	30	14.4	17756.0	-	-
	2	30	15.1	18068.1	-	-
Type-A CNT (Nucleate Boiling)	1	30	16.4	41284.1	128.49	132.51
	2	30	15.7	41986.3	132.38	136.46
Type-B CNT (Nuc. Boiling)	1	30	17.7	33596.1	85.94	89.21

Table A-7

Continued.

Test Surface	Run	Subcooling Level (°C)	Wall Superheat (°C)	Heat Flux (W/m^2)	Percent Improvement (Min)	Percent Improvement (Max.)
Bare Silicon (Near CHF)	1	30	54.5	50844.7	-	-
	2	30	46.4	45203.7	-	-
Type-A CNT (Near CHF)	1	30	28.9	63260.7	24.42	39.95
	2	30	27.5	63546.4	24.98	40.58

Table A-8

Non-departing bubble condition.

Test Surface	Run	Subcooling Level (°C)	Heat Flux (W/m^2)	Uncertainty (%)
Bare Silicon (Near CHF)	1	~ 38*	30770.0	13.98
Type-A CNT (Near CHF)	1	~ 33.0	39429.8	11.50
	2-1	~ 34.5	38684.7	10.54
	2-2	~ 33.0	38852.2	13.30

* Temperature for this point was measured with NIST thermometer as thermocouple measuring the liquid temperature failed.

VITA

Name: Vijaykumar Sathyamurthi

Address: Department of Mechanical Engineering,
Texas A&M University,
College Station,
Texas – 77843-3123

Education: M.S., Mechanical Engineering, Texas A&M University,

Dec. 2006.

B.E. (Honors), Mechanical Engineering, Nagpur University,

Aug. 2003.

Publications:

[1] H. Ahn, V. Sathyamurthi, N. Sinha, S. Lau and D. Banerjee, Boiling Experiments on Vertically Aligned Carbon Nanotubes and using Surface Micromachined Thin Film Thermocouple (TFT), AIAA-2006-2916, 36th, AIAA Fluid Dynamics Conference San Francisco, CA, June 5–8, 2006.

[2] V. Sathyamurthi, D. Banerjee, Highly Subcooled Pool Boiling on Nano-Textured Surfaces, Advanced Technology Workshop on Thermal Management, IMAPS-2006, Palo Alto, CA, September 10-13, 2006.